AD-A051 344 SRI INTERNATIONAL MENLO PARK CA F/G 17/9
RADAR TRACKING OF ION CLOUDS. TECHNICAL REPORT 1 - PROJECT STRE--ETC(U)
JUL 77 V H GONZALEZ DNA001-76-C-0341
UNCLASSIFIED DNA-4373Z NL

| OF |
AD
A051344

END
DATE
FILMED
4 -78
DDC

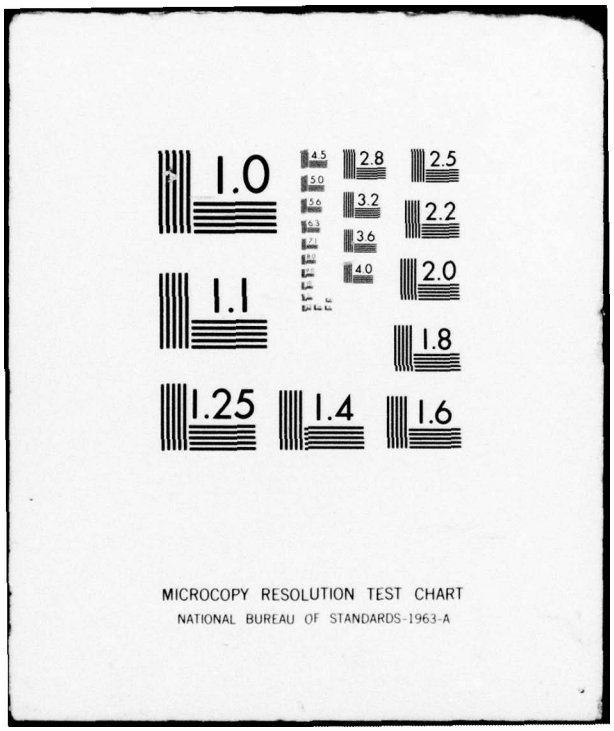
1.0
1.1
1.25
1.4
1.6
1.8
2.0
2.2
2.5
2.8
3.2
3.6
4.0
4.5
5.0
5.6
6.3
MICROCOPY RESOLUTION TEST CHART
NATIONAL BUREAU OF STANDARDS-1963-A

(6)

RADAR TRACKING OF ION CLOUDS.

Technical Report 1-Project STRESS.

(12)

SRI International
333 Ravenswood Avenue
Menlo Park, California 94025

(10) Victor H. Gonzalez

(11) Jul[redacted]77 (12) 55 p.

(9) Interim Report, [redacted] Jul[redacted]76—Mar[redacted]77,

CONTRACT No. DNA 001-76-C-0341

(15)

APPROVED FOR PUBLIC RELEASE;
DISTRIBUTION UNLIMITED.

THIS WORK SPONSORED BY THE DEFENSE NUCLEAR AGENCY
UNDER RDT&E RMSS CODE B32207T462 L25AAXHX63512 H2590D.

Prepared for
Director
DEFENSE NUCLEAR AGENCY
Washington, D. C. 20305

Destroy this report when it is no longer needed. Do not return to sender.

UNCLASSIFIED

SECURITY CLASSIFICATION OF THIS PAGE *(When Data Entered)*

REPORT DOCUMENTATION PAGE		READ INSTRUCTIONS BEFORE COMPLETING FORM
1. REPORT NUMBER DNA 4373Z	2. GOVT ACCESSION NO.	3. RECIPIENT'S CATALOG NUMBER
4. TITLE *(and Subtitle)* RADAR TRACKING OF ION CLOUDS Technical Report 1—Project STRESS		5. TYPE OF REPORT & PERIOD COVERED Interim Report for Period July 1976—March 1977
		6. PERFORMING ORG. REPORT NUMBER SRI Project 5575
7. AUTHOR(s) Victor H. Gonzalez		8. CONTRACT OR GRANT NUMBER(s) DNA 001-76-C-0341
9. PERFORMING ORGANIZATION NAME AND ADDRESS SRI International 333 Ravenswood Avenue Menlo Park, California 94025		10. PROGRAM ELEMENT, PROJECT, TASK AREA & WORK UNIT NUMBERS Subtask L25AAXHX635-12
11. CONTROLLING OFFICE NAME AND ADDRESS Director Defense Nuclear Agency Washington, D.C. 20305		12. REPORT DATE July 1977
		13. NUMBER OF PAGES 62
14. MONITORING AGENCY NAME & ADDRESS *(if different from Controlling Office)*		15. SECURITY CLASS *(of this report)* UNCLASSIFIED
		15a. DECLASSIFICATION/DOWNGRADING SCHEDULE

16. DISTRIBUTION STATEMENT *(of this Report)*

Approved for public release; distribution unlimited.

17. DISTRIBUTION STATEMENT *(of the abstract entered in Block 20, if different from Report)*

18. SUPPLEMENTARY NOTES

This work sponsored by the Defense Nuclear Agency under RDT&E RMSS Code B32207T462 L25AAXHX63512 H2590D.

19. KEY WORDS *(Continue on reverse side if necessary and identify by block number)*

Barium Releases
Ion-Cloud Tracking
Incoherent-Scatter Measurements
UHF Radar

20. ABSTRACT *(Continue on reverse side if necessary and identify by block number)*

Project STRESS utilized a series of high-altitude releases of barium that became ionized by solar radiation. The project required that the resulting ion cloud be tracked in real time, and this was accomplished by operating the AN/FPS-85 radar in the incoherent-scatter mode. This report describes the data-acquisition process and the tracking algorithm, and presents a preliminary look at the most important measurements obtained. The tracking of a Ba-ion cloud, attempted for the first time, was successfully accomplished for the time periods of up to 10 minutes.

DD FORM 1 JAN 73 1473 EDITION OF 1 NOV 65 IS OBSOLETE

UNCLASSIFIED

SECURITY CLASSIFICATION OF THIS PAGE *(When Data Entered)*

CONTENTS

ILLUSTRATIONS

I INTRODUCTION

STRESS (Satellite Transmission Effects Simulation) is a communication experiment that took place between November 1976 and March 1977 and was sponsored by the Defense Nuclear Agency (DNA) in cooperation with the Air Force Electronic System Division (ESD). The purpose of the experiment was to gather data with which to evaluate the reliability of satellite communications under conditions that simulate many aspects of an environment that follows a nuclear burst. The environment was produced by the use of ionospheric releases of barium, placed so that the communication path from a synchronous satellite (LES-8 or LES-9) to an airborne receiving station passed through the barium ion cloud. The real-time track of the cloud was provided by two means: low-light-level TV, and radar (we used the AN/FPS-85 radar located at Eglin AFB).

The prime objective of the radar track of the high-altitude Ba-ion cloud was to guide the airborne receiving station into the shadow of the cloud in order to attain an occulted aircraft-to-satellite propagation link. The secondary objective of the experiment was to obtain data from the ion cloud for diagnostic purposes so the electron density in space and time could be described.

II BACKGROUND

The AN/FPS-85 radar is a high-powered phased-array UHF radar. It transmits horizontally polarized pulses in a beam 1.6° wide and receives the echoes in up to nine beams, each 0.8° wide in both vertical and horizontal polarizations. During STRESS, the radar operated in an incoherent (Thompson) scatter mode in which signal returns were reflected by free electrons in the beam path. By suitable scanning of the beam in azimuth and elevation, the region of maximum electron density was identified and tracked and the data were recorded.

The electrons reflect EM energy individually, and because their arrangement in space and also their velocities are completely random the reflected signal has the same statistical properties as noise. The detected signal is Rayleigh distributed and the instantaneous sampled power (square of the detected signal amplitude) is random and exponentially distributed.

When the electron density of a volume in space is to be measured by the incoherent-scatter technique, we point the radar beam to that particular volume and determine the average power returned from it by using several pulses and averaging the returns. Contrary to a hard target echo, a single return from free electrons provides us with little, if any, information about the radar cross section we wish to measure, even though the signal-to-noise ratio (SNR) may exceed 25 dB. A sample average must always be obtained.

With the foregoing consideration in mind we shall discuss various topics related to the measurements being performed.

A. Waveform, Sensitivity, and Measurement of Electron Density

The SNR from the incoherent-scatter echoes of a beam-filling, ionized medium with electron density N is given by the following equation

$$\frac{P_s}{P_N} = \frac{K_s N}{R^2}\left(1 + \frac{T_e}{T_i}\right) \tag{1}$$

where K_s is a system parameter that is different for each waveform and that incorporates all the radar characteristics, and

P_s = Received signal power

P_N = System noise power

R = Range

T_e/T_i = Ratio of electron to ion temperature.

P_s is proportional to the transmitted energy in each pulse and P_N is proportional to the reciprocal of the pulse length, so a tradeoff exists between SNR and range resolution when choosing a waveform. Figure 1 shows the SNR that can be attained with the most important waveforms available in the AN/FPS-85. The 250/10-μs compressed pulse is seen to be the waveform with the highest available SNR. The range resolution inherent in the 10-μs compressed pulse is 1.5 km.

The accuracy of the measurement of N depends on the accuracy with which the received power $P_R = P_s + P_N$ can be measured. If J independent measurements are averaged to measure $\bar{P}_R$, the standard deviation of the sample mean $\bar{P}_R$ is $\sigma_R = \bar{P}_r/\sqrt{J}$ and the accuracy attainable in the determination of P_s is

$$\frac{\sigma_s}{P_s} = \frac{\sigma_R}{P_s} = \frac{1 + SNR}{(SNR)\sqrt{J}} \quad . \tag{2}$$

For a reasonably large SNR (5 dB or more) the attainable accuracy is mainly a function of the number of independent measurements, J, used for the averaging. J is the number we wish to maximize, and the independent measurements that are counted in J can be made on different pulses at the same range, contiguous range cells in the same pulse (10 independent measurements every 150 m would give a good sample average every 1.5 km), or both. For this reason, even though the 128/10-μs compressed pulse achieves a smaller SNR than the 250/10-μs pulse, the PRF is twice as great. Thus, for equal integration time, J can be twice as

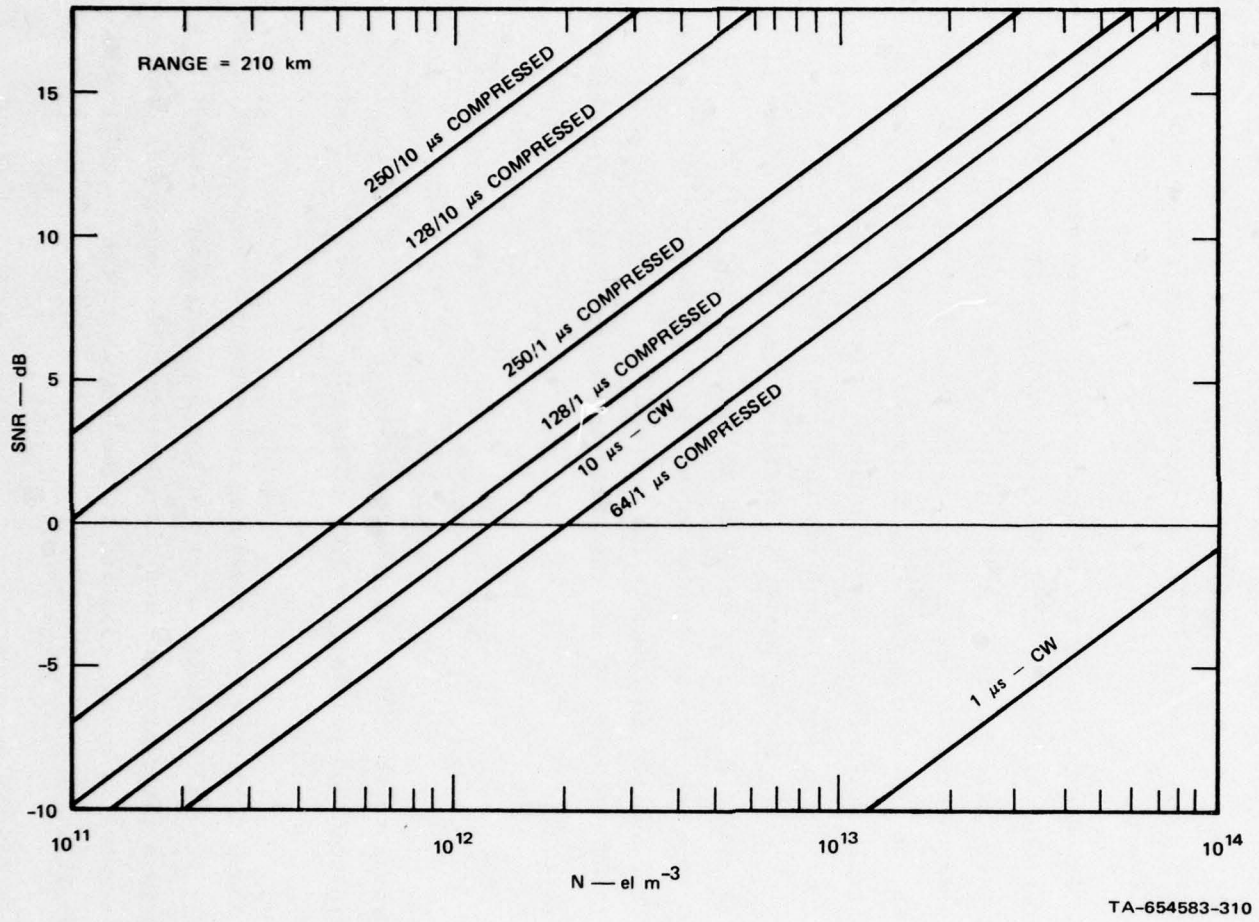

FIGURE 1 EXPECTED SIGNAL-TO-NOISE RATIO vs ELECTRON DENSITY EXPECTED FOR VARIOUS WAVEFORMS

large as it would be if the 250/10-μs compressed pulse were used. The use of the 250/1-μs compressed waveform would be still more advantageous if the sampling rate could be increased to take full advantage of the range resolution. Since the sampling rate of the A/D converters is limited to one sample every 5 μs, the 128/10-μs compressed pulse was chosen as the most suitable.

In addition to the accuracy of measurement, we are also concerned with the detectability of an echo above the noise level. In the case of detecting hard targets using a single pulse, 10 to 14 dB above noise level is considered a reliable threshold. In the noise-like case we are concerned with, we should remember that the average noise power $\overline{P}_N$ can be very accurately determined. When we measure a sample mean $\overline{P}_R = \overline{P}_s + \overline{P}_{Ns}$, the sample mean $\overline{P}_{Ns}$ should be substracted from $\overline{P}_R$ to obtain $\overline{P}_s$; the sample mean $\overline{P}_{Ns}$ is not known, and it is different from $\overline{P}_N$ even though its expectation equals $\overline{P}_N$ and its standard deviation is $\sigma_{Ns} = \overline{P}_N/\sqrt{J}$. The quantity σ_{Ns} is the effective noise level, and is the quantity that would determine our ability to identify the presence of a detectable echo. Thus, if 10 dB is chosen as the threshold noise, the detectable signal power is given by

$$\overline{P}_s \geq 10 \frac{\overline{P}_N}{\sqrt{J}} \quad . \tag{3}$$

According to the 128/10-μs compressed-pulse curve given in Figure 1, we would need 100 pulses (J = 100) to be able to detect 10^{11} electrons m^{-3}.

The above considerations regarding measurement accuracy [summarized by Eq. (2)] led to the design of one of the tracking modes (Mode I) described in a later section; and the considerations concerning detectability [summarized by Eq. (3)] led to the design of the second tracking mode (Mode II).

B. Temperature Ratio

In the analysis of the SECEDE II data,* good agreement was found between the electron densities obtained from Faraday rotation data and those from incoherent-scatter data by assuming a temperature ratio equal to 1. This fact indicates that the T_e/T_i ratio is not appreciably larger than 1. We intend to check this assumption during analysis of the STRESS data.

C. Angular and Range Resolution

The AN/FPS-85 radar transmits energy in a single main beam whose 3-dB beamwidth is approximately 1.6°. A separate antenna array used for receiving forms a 3-by-3 array of beams positioned 0.40° apart. Each of these nine receiver beams has a 0.8°, 3-dB width. Figure 2 is a diagram of the angular coverage of the radar, showing the transmitting beam and the five receiving beams closest to the center of the transmitting beam. At nominal ion cloud range of about 200 km, an angular resolution equivalent to 2.5 km is achieved.

The range resolution inherent in a 128/10-μs compressed pulse is 1.5 km; thus, we may think of an elemental scattering volume as a cylinder 2.5 km in diameter and 1.5 km thick. The electron densities measured by the radar averages over such a volume and we can expect to measure no finer detail. For tracking purposes the central beam was used exclusively; however, data from the west receiving beam were also recorded for post-experiment analysis.

D. Polarization

The AN/FPS-85 transmits in horizontal polarization and receives in both vertical and horizontal polarizations. The echoes are subjected to Faraday rotation by the ionized ion cloud and the natural ionosphere in presence of the natural earth magnetic field, so that both polarizations have to be received, processed, and recorded in parallel.

*References are listed at the end of the report.

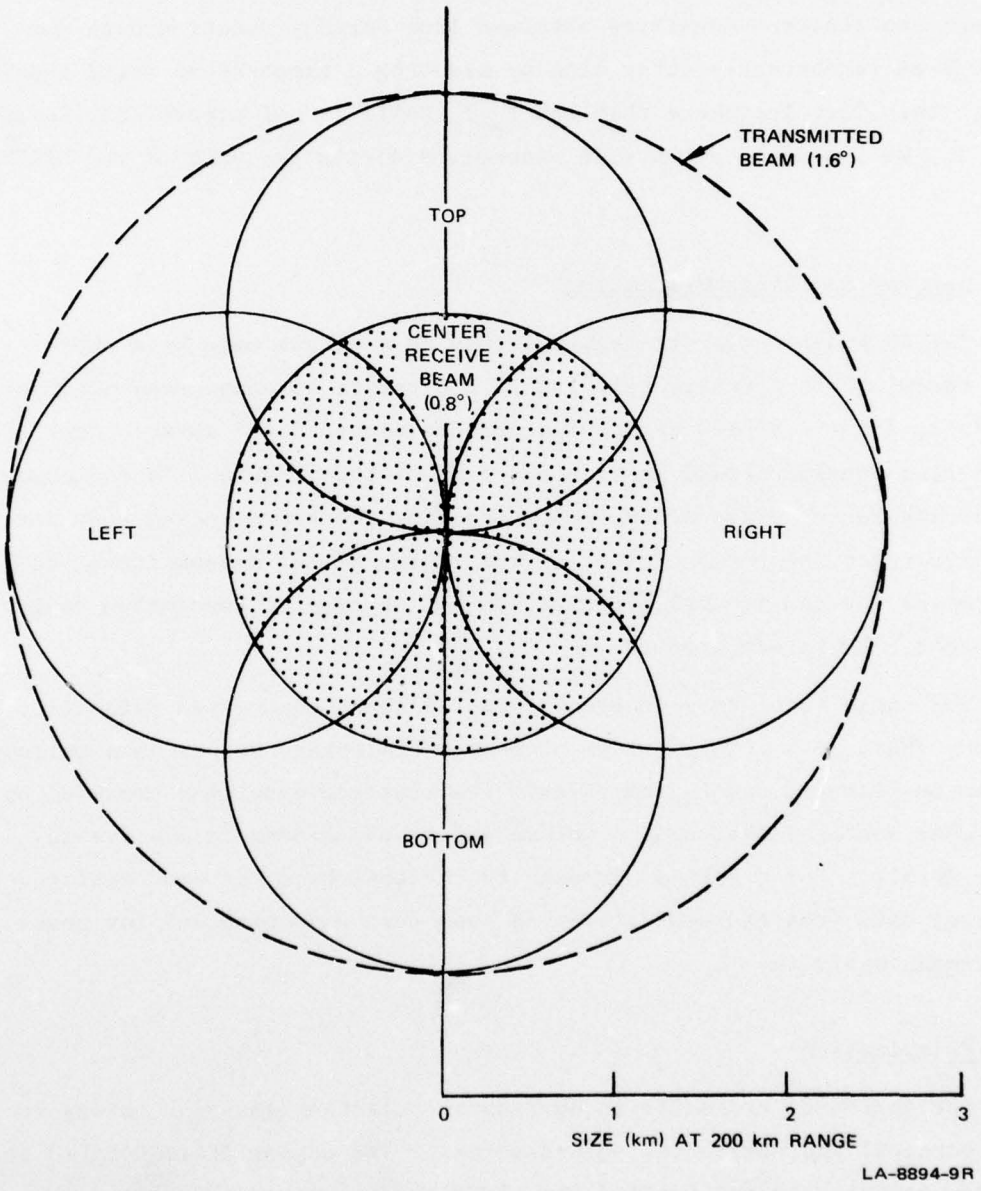

FIGURE 2 ANGULAR COVERAGE (3-dB beams)

The Faraday rotation effect has been used in the past to yield electron densities. As mentioned above, it could be used as a means of calibrating the system constant, K_s, of the radar and/or verifying the temperature ratio, T_e/T_i.

E. Calibration of the Radar

Two aspects of calibration have to be addressed. One is the determination of the receiver response law, or curve, and the other is the determination of the constant K_s of Eq. (1).

The receiver response curve describes the correspondence between the numbers fed to the computer by the A/D converters and the power received by the antenna array. Receiver response curves, one for each polarization, are shown in Figure 3 as A/D converter readings, versus the ratio P_s/P_N, where P_N is the system noise, as before, and P_S is the power backscattered by the free electrons. The lower ends of the curves of Figure 3 were determined by analyzing about 5×10^5 samples of system noise, and an equal number of samples of system noise plus a noise source. These samples allowed calibration over a dynamic range of about 40 dB; this range is shown in Figure 3. The upper portions of the curves, which extend to A/D converter readings of 256, were extrapolated by the logarithmic characteristic of the amplifiers, which is 0.25 dB per A/D converter increment step. The upper part of the curve is routinely measured in the AN/FPS-85 by using pulses, but the lower part of the curve (shown in Figure 3) is not, even though it was very important to our task.

The determination of the constant K_s of Eq. (1), which incorporates all the other system characteristics such as power transmitted and antenna gains, is the second step in the calibration of the radar. The values of the maximum electron density of the natural F-layer measured simultaneously by an ionosonde and the AN/FPS-85 provide an absolute scale between P_s/P_N and N as expressed by Eq. (1).

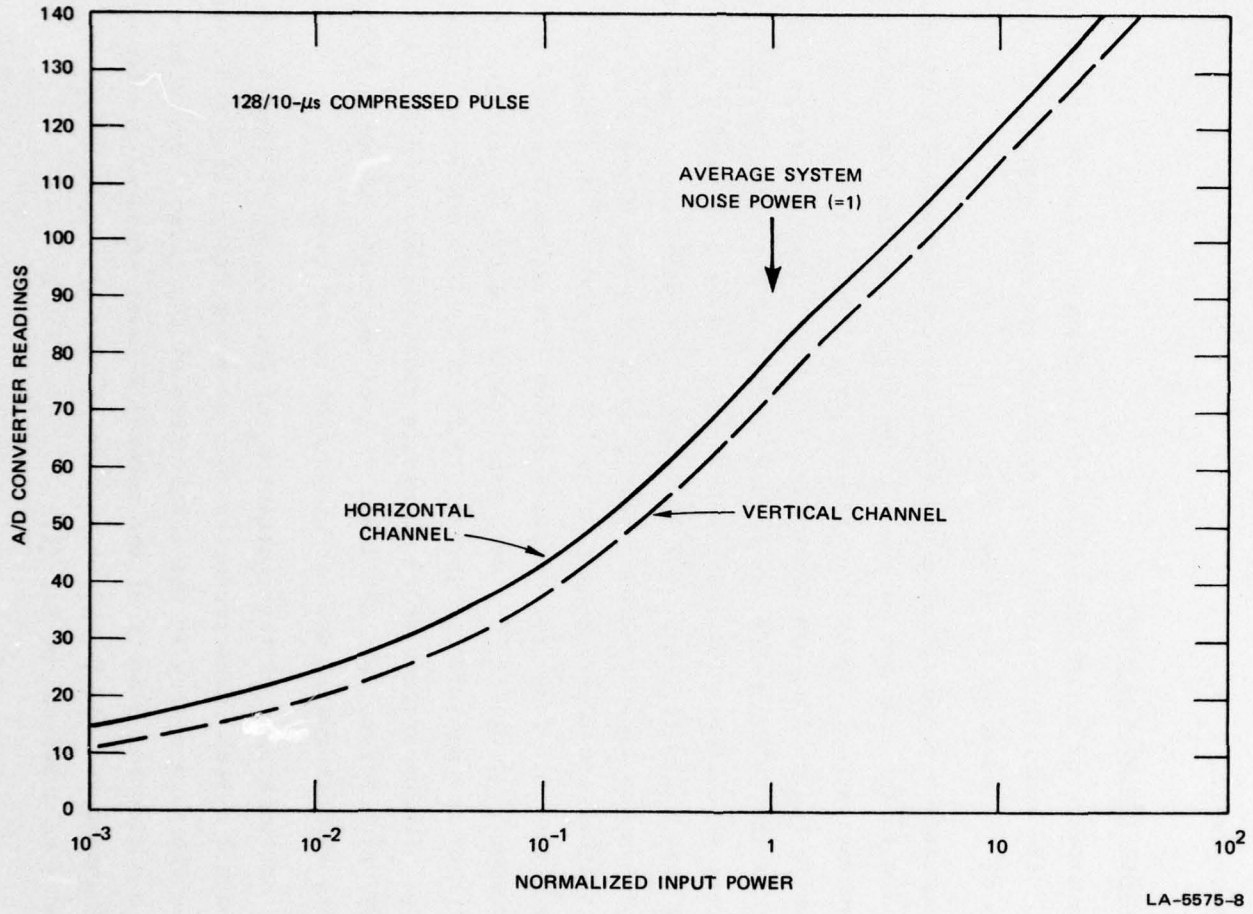

FIGURE 3 RECEIVER RESPONSE CURVES

III DATA ACQUISITION AND PROCESSING

A. Signal Sampling

Since the AN/FPS-85 is an operational radar whose function is to track point targets, it has several features in its logic that ensure that the measurements will be acquired at the peaks of return signals. The signal to be measured using the incoherent-scatter technique, on the other hand, has to be sampled at fixed ranges from pulse to pulse at least during an integration period or pulse group, and the sampling has to be performed regardless of whether it is at a peak, a valley, or in between. The requirement is that each sample should be statistically independent from the rest of the samples acquired.

In order for the sampling to be done according to our specifications, a combination of software instructions and hardware modifications was implemented. For each transmitted pulse, a computer-generated raster of "sample pulses" was sent to the signal-processor area to cause the samples to be read out into the computer/radar interface every 10 μs between a start range, R_1 (145 km for event ANNE, 130 km for the other events), and an end sampling range, R_2 (400 km and 385 km, respectively). A total of 171 samples was taken in that range interval, giving 170 cells. In addition to the above, 40 samples were acquired at a range of about 3000 km; 20 of these samples were used to monitor variations in the system noise and the other 20 samples were acquired when a constant noise source was injected into the receiving electronics so as to monitor variations in the characteristics of the receiver-amplifier chain.

The A/D converters in their normal operation sample the output of the receivers continuously at a very high rate, so the raster of computer-generated pulses actually gave the command of reading the latest sample into the RICE (Radar/computer interface) and into the computer. A built-in peak-hold feature of the A/D converters had to be disabled to ensure

that the acquired samples were instantaneous, uncorrelated, and representative of a Gaussian noise process.

Two additional pulses were generated by computer to turn on and off a noise source generator that was coupled to the receiving system through a balanced coupler. The noise source was on for 175 μs at a delay, equivalent to 3050 km, from the transmitted pulse.

B. Data Acquisition

The basic block of data was obtained while the radar was pointing in a fixed direction for periods of time that varied between 1 and 5 s. During these periods, the 128/10-μs compressed pulse was transmitted at a PRF of 40 pps. The returned noise-like signal of each pulse was sampled as explained in Section III-A, above, in each of the two polarizations of two of the receiving beams (main beam and west beam). In Figure 4 we call the set of 171 horizontal polarization samples X_H, and the set of 171 vertical polarization samples X_V.

With the use of the receiver response curve that was stored in the memory, the values X_H and X_V were converted into $(P_s + P_N)/P_N$ levels Y_H and Y_V. It is the values Y_H and Y_V that are averaged for each range cell over all the pulses used in the 1-to-5-s period. The result is 171 values of $\bar{Y}_H$ and 171 values of $\bar{Y}_V$. Figure 5 shows, as a function of range, the curves $\bar{Y}_H + \bar{Y}_V$ that were obtained during one of the events. The values of $\bar{Y}_H$ and $\bar{Y}_V$ corresponding to the main beam and the west beam were recorded on magnetic tape for post-experiment analysis.

During the first 30 s after release of the barium, the individual values of X_H and X_V were recorded as rough data on a pulse-by-pulse basis, without any integration for later analysis. During these 30 s, no effort was made to track the cloud, so the recording at a large data rate was possible.

C. Real-Time Data Processing

The data processing in real time was performed for the main beam only and it was oriented to find the data required for tracking of the

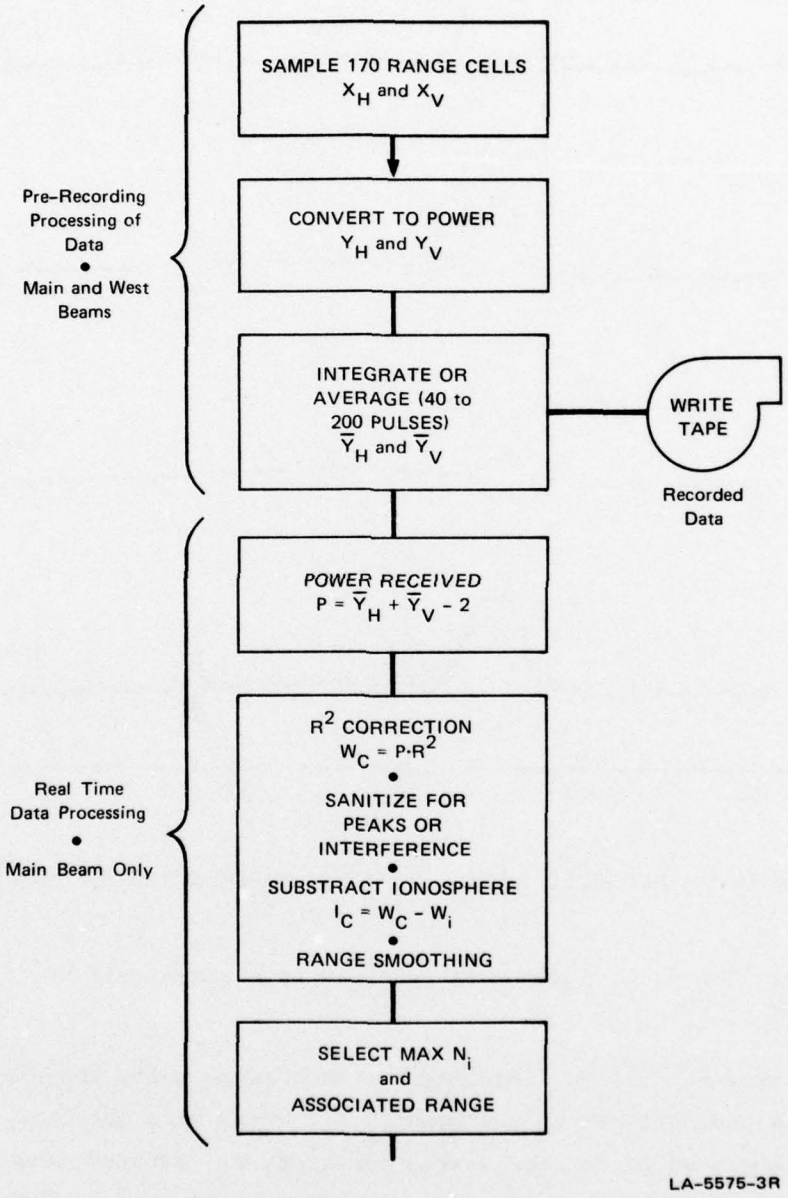

FIGURE 4 BASIC BLOCK OF DATA — 1-TO-5-s INTEGRATION TIME AT CONSTANT AZIMUTH AND ELEVATION

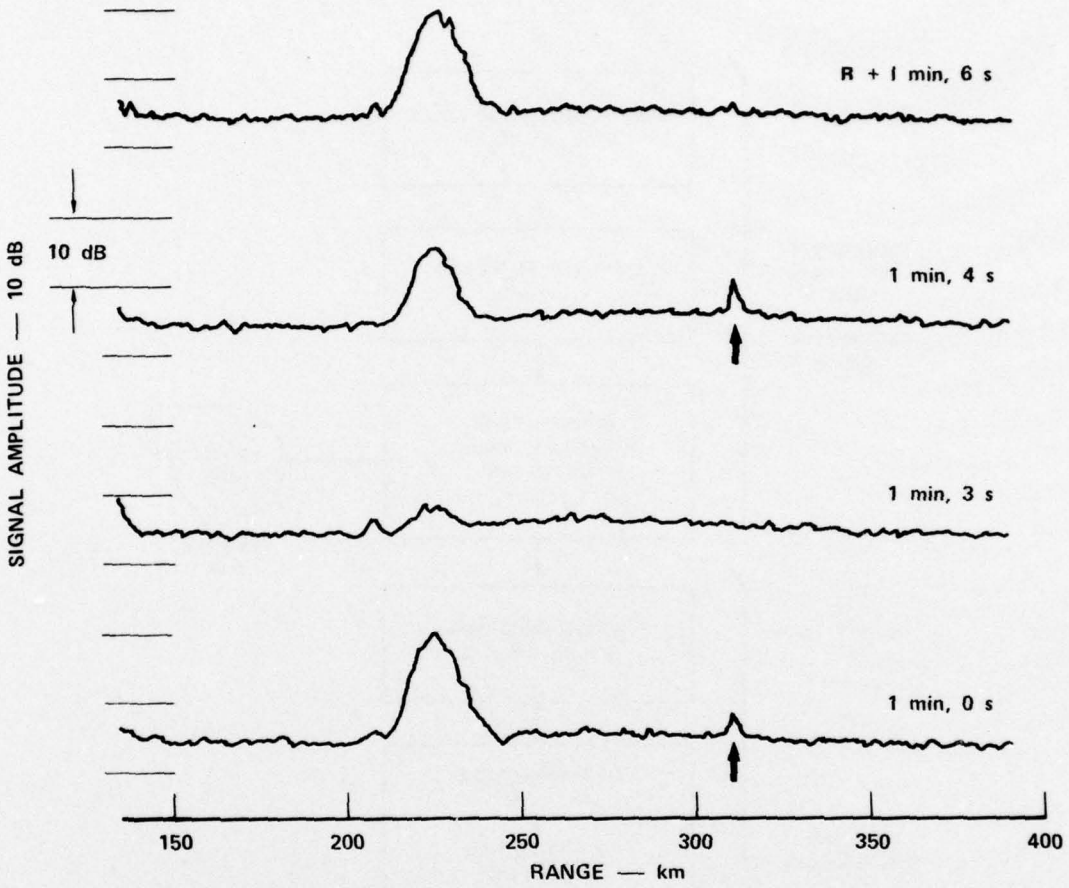

FIGURE 5 RECORDED DATA — $\bar{Y}_H + \bar{Y}_V$ AS A FUNCTION OF RANGE

ion-cloud. The total power received from each range cell is $P = \bar{Y}_H + \bar{Y}_V - 2$.

By using Eq. (1) we find that for each range cell, the electron density is proportional to the numbers i_c, which were obtained by using an approximate value for the system constant, K_s, deduced from Figure 1. An accurate determination of K_s is not necessary during tracking; only an approximate value is required.

In the curve of Event ANNE we found that interference spikes occurred frequently and were extremely misleading to the tracking logic, so we

developed and implemented a software algorithm to sanitize narrow spikes in the data of the remaining events. Furthermore, a triangular convolution filter was also used to smooth out the range variation of the data.

Examples of the values i_c (electron densities) as a function of range are shown in Figure 6. The maximum value of i_c (N_m), the range at which that value occurred (R_m), and the azimuth and elevation of the beam for each particular block of data are the four numbers that summarize the results of real-time data processing of a single beam position of the antenna. These values were transferred to the tracking algorithm, explained in the next section.

D. Additional Data

The data acquired to obtain the receiver response curves as explained in Section II-E and the data acquired to measure the ionosphere were also recorded for later detailed analysis.

The ionosphere runs consisted of acquiring data similar to ion-cloud data with longer integration times (15 seconds to 4 minutes) and with the radar beam pointing to regions free of barium ions. Figure 4 shows the sequence of operations followed except that the step "Substract Ionosphere" is absent; actually, we determine the array W_i to be substracted from the ion cloud data.

The ionosphere runs also provided data to determine the constant K_s of Eq. (1) as discussed in Section II-E.

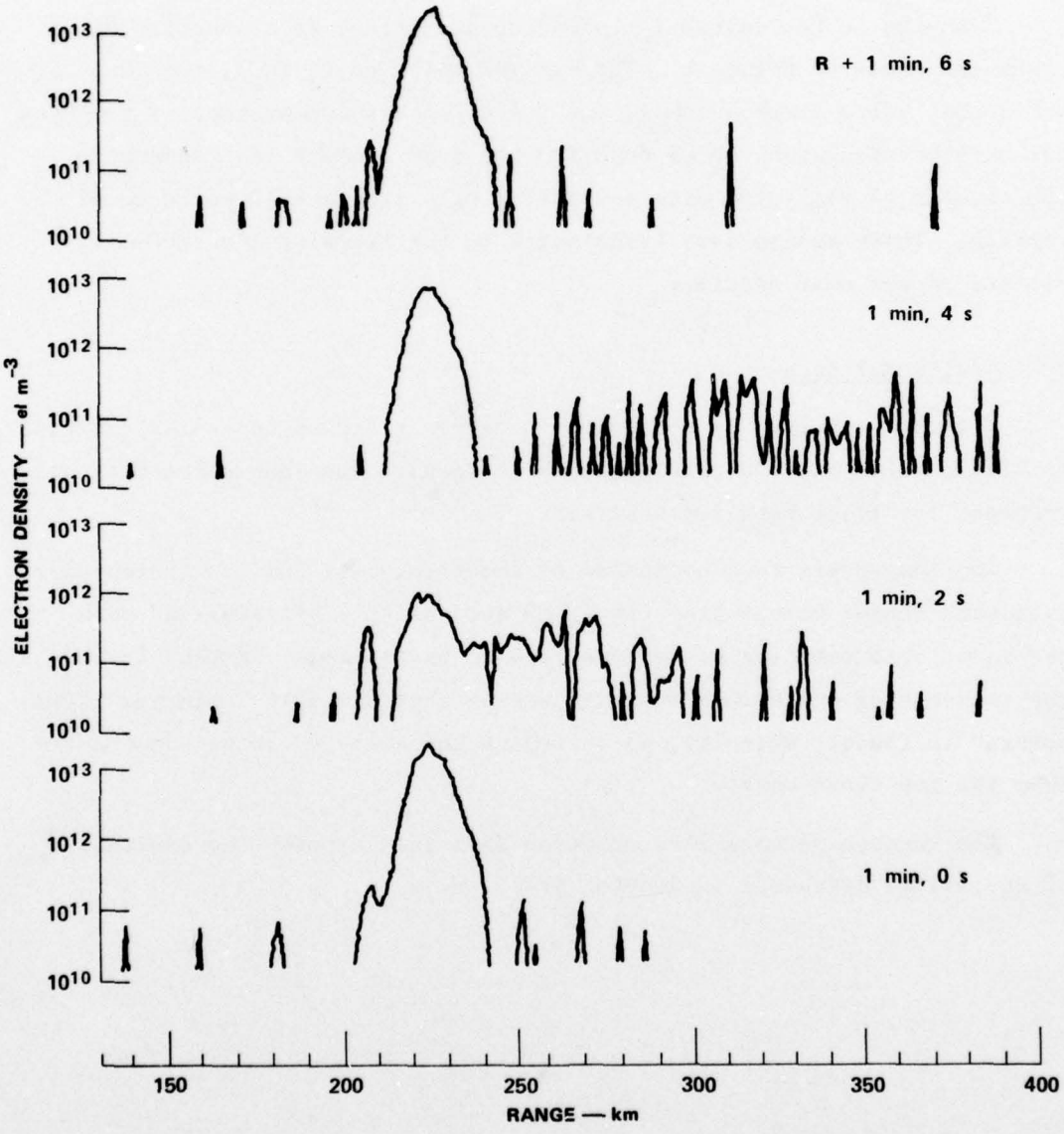

FIGURE 6 PROCESSED DATA — $i_c \times 10^{11}$ AS A FUNCTION OF RANGE

IV TRACKING ALGORITHM

The tracking algorithm consists of the circular logic shown in Figure 7. Having an estimate of the ion-cloud position, the radar points and acquires data at and around that position. From these data it determines a measured position of the cloud. The new measured position of the ion cloud is used in a tracking recursive filter that averages the new measurement with previous measurements and yields an updated estimate that is used to re-start the cycle. The cycle is initialized by tracking the payload rocket and recording its position at the nominal time of release.

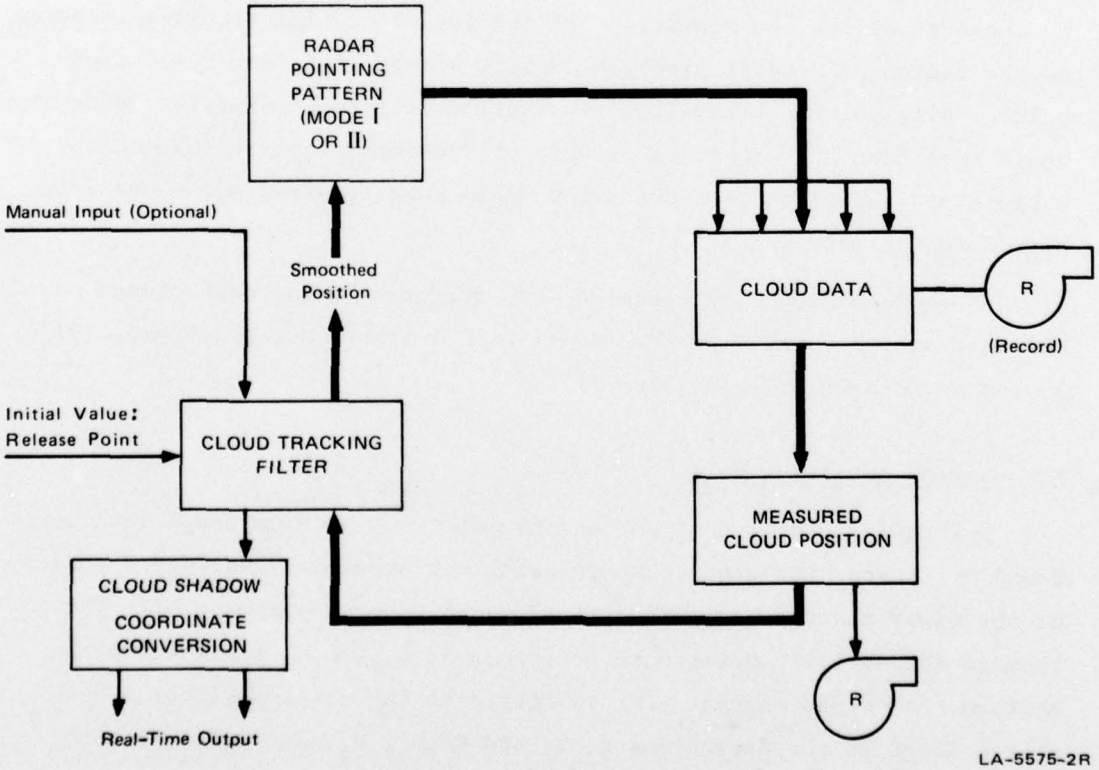

FIGURE 7 CLOUD-TRACKING LOOP

There were several choices to make in the design of the tracking logic; the most relevant and difficult were:

(1) Pattern of pointing directions around the estimated position

(2) Integration time in each position

(3) Analytic definition of a measured ion-cloud position.

We required three characteristics in the tracking algorithm that happen to conflict with each other:

(1) Speed and simplicity of computations.

(2) Accurate electron density measurements.

(3) Measurements that are short enough in time so the ion cloud can be considered stationary.

The analytic definition of the position of the ion cloud seems quite simple at early times after release; however, at later times the examination of a picture shows that this definition can be very complicated. We chose to define the "position" of the ion cloud, for tracking purposes, as the region of highest electron density within a minimum-resolution volume cell, which was explained in Section II. An alternative definition could have been the center of gravity of the ionization throughout the whole cloud; however, this criterion would have required much more extensive computations.

In terms of scanning patterns, two different modes were chosen as the most satisfactory. The two modes were a strobe autotrack mode (Mode I) and a rectangular scan (Mode II).

A. Strobe Autotrack Mode

The basic operation of the strobe autotrack mode is shown in Figures 8 and 9. A scanning plane that contains the previously estimated position of the cloud and the radar is defined by an angular parameter β. The beam is sequentially pointed to positions A, B, and C, separated by an angle α. A second-degree curve is fitted to the maximum electron densities found in the directions A, B, and C (N_A, N_B, and N_C), and both the "measured" center of the cloud and a projected width of the cloud

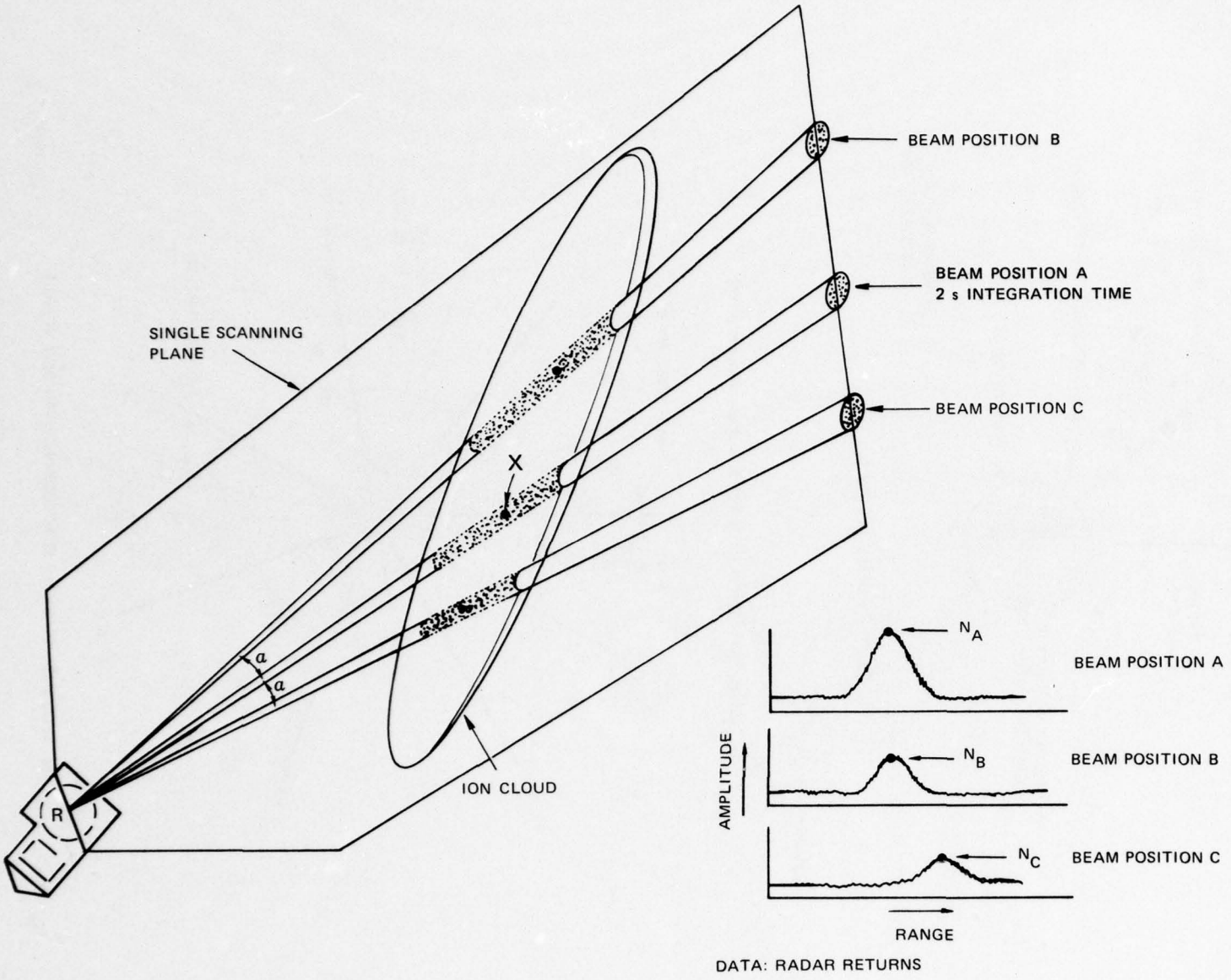

FIGURE 8 THREE MEASUREMENTS PERFORMED IN A SINGLE SCANNING PLANE

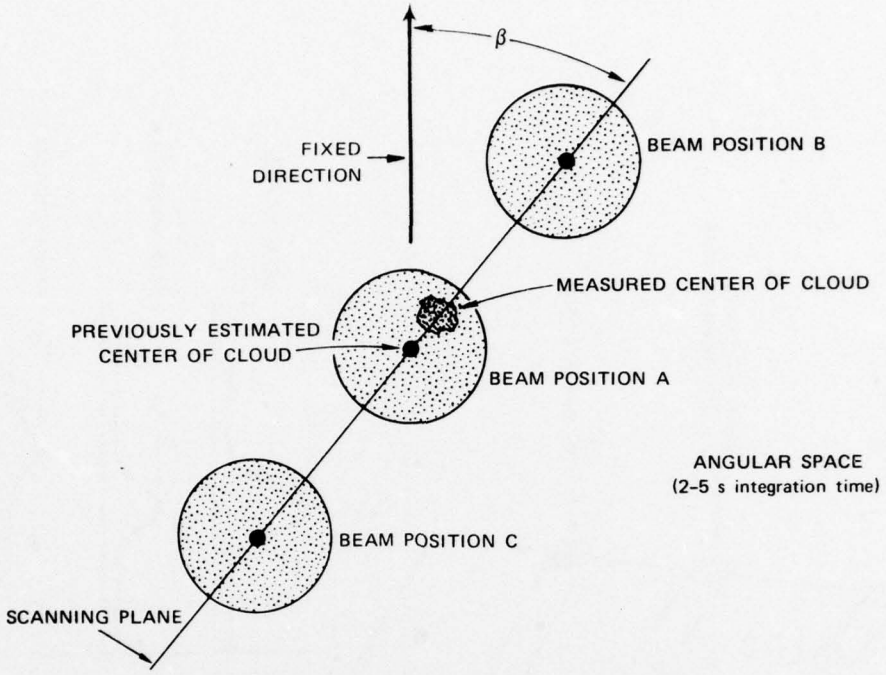

(a) BASIC OPERATION OF MODE I (a single scanning plane)

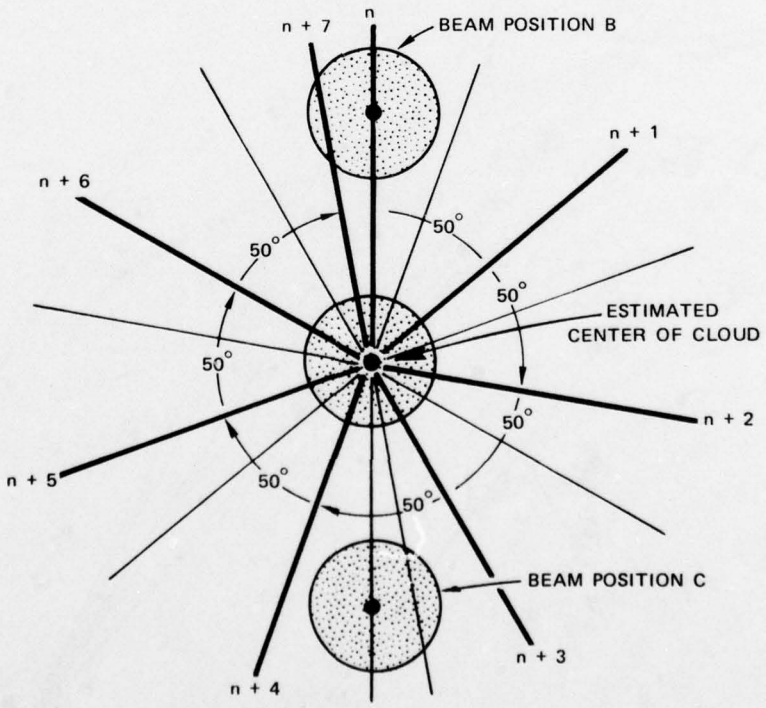

(b) SEQUENCE OF EIGHT CONSECUTIVE SCANNING PLANES

LA-5575-5

FIGURE 9 STROBE AUTOTRACK MODE (Mode 1)

are found from the fitted curve. The measured center of the cloud is assigned to the maximum value of the fitted curve, and the projected width is chosen at one-fourth of the maximum electron density. The measured position is then fed to the tracking filter and the projected width of the cloud is saved in the memory to adjust the beam separation α the next time the same scanning plane is used.

After the measurement in a single scanning plane is completed and used in the tracking filter, the scanning plane is rotated 50° around the line RX of Figure 8, and the procedure is repeated.

Figure 9(b) shows in angular space a sequence of eight consecutive scanning planes around the center of the cloud, and it can be seen that 18 successive scanning planes would perform measurements in all positions, every 10° around the cloud.

Figure 10 shows the position scanned in one minute by this mode of operation. The center position has been repeated several times.

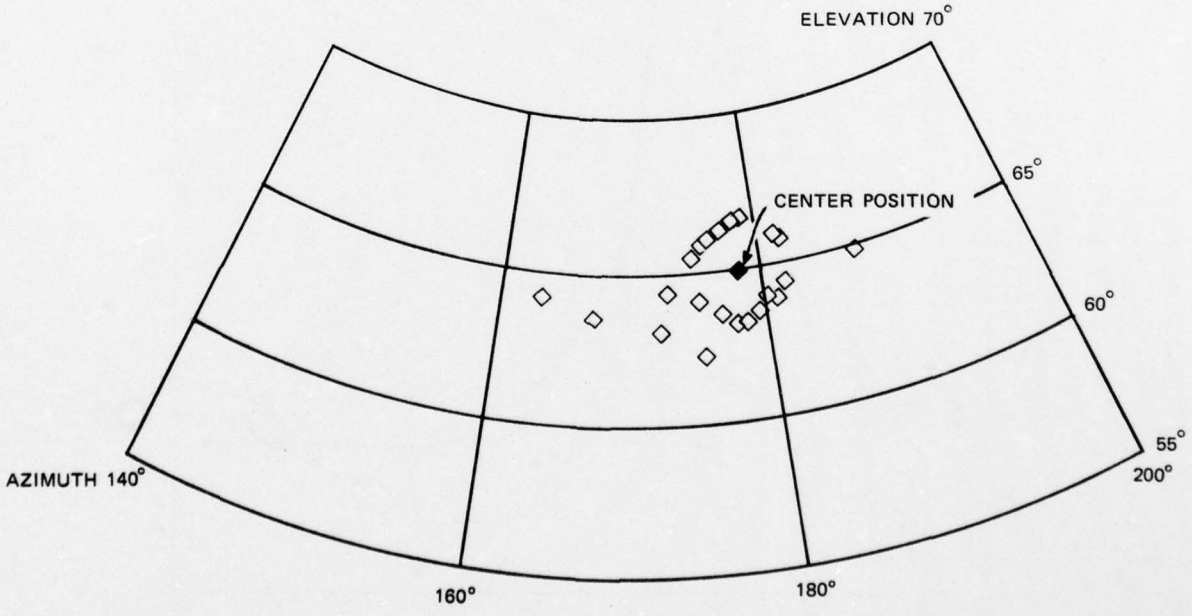

FIGURE 10 DIFFERENT DIRECTIONS IN WHICH THE RADAR BEAM WAS POINTED DURING 1 MINUTE OF MODE 1 TRACKING — EVENT ANNE

The scanning of Mode I attempted to define the shape of the cloud, and the emphasis of this mode is in measurement accuracy. The integration times were chosen in accordance with Eq. (2) to attain 10% accuracy. This mode of operation worked extremely well and was used primarily.

Figure 11 shows a plot of the projected width of the clouds as a function of β. In this example $\beta \approx 0$ corresponds approximately to the direction toward the zenith.

B. Rectangular Mode

The rectangular scanning mode (Mode II) is an ordinary rectangular array of a variable number of up to 40 beam positions, as is shown in

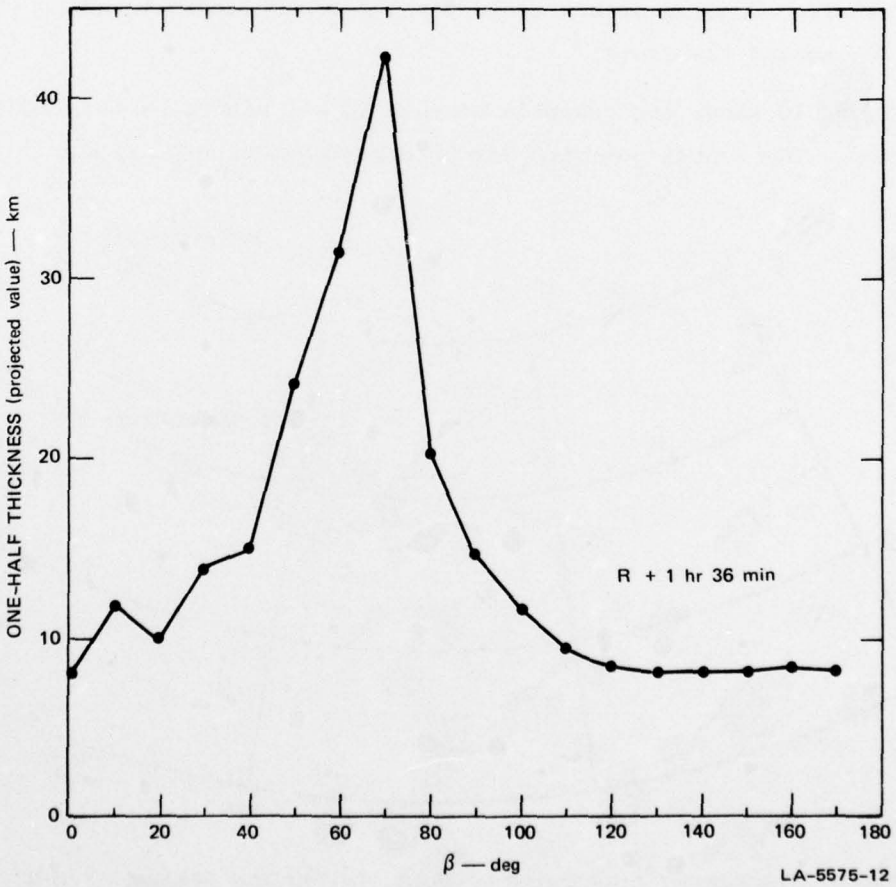

FIGURE 11 PROJECTED WIDTH OF ION CLOUD AS A FUNCTION OF β — EVENT ANNE

Figure 12. The rectangular pattern is defined by an angle β, which was selected to correspond to the maximum value of the projected width as obtained with Mode I. The array spacings, ΔA and ΔB, are also related to the measured projected widths. Initially Mode II was implemented as a 5-by-5 array, as shown in Figure 12.

The measured cloud position was simply the location of the maximum value of electron density found in all the scans. The emphasis of this mode is on detectability, so the integration times were adjusted to permit detection of 10^{11} el/m^3 at a range of 210 km.

A further use of this mode is the acquisition of data from a large portion of the Ba-ion cloud including areas of marginal ionization and even points with no cloud at all.

C. Tracking Filter

The tracking filter used was a simplified sequential-type Kalman filter that used each measurement only once. This filter was designed to erase gradually the statistical weight of all measurements so that changes in direction of drift can be followed.

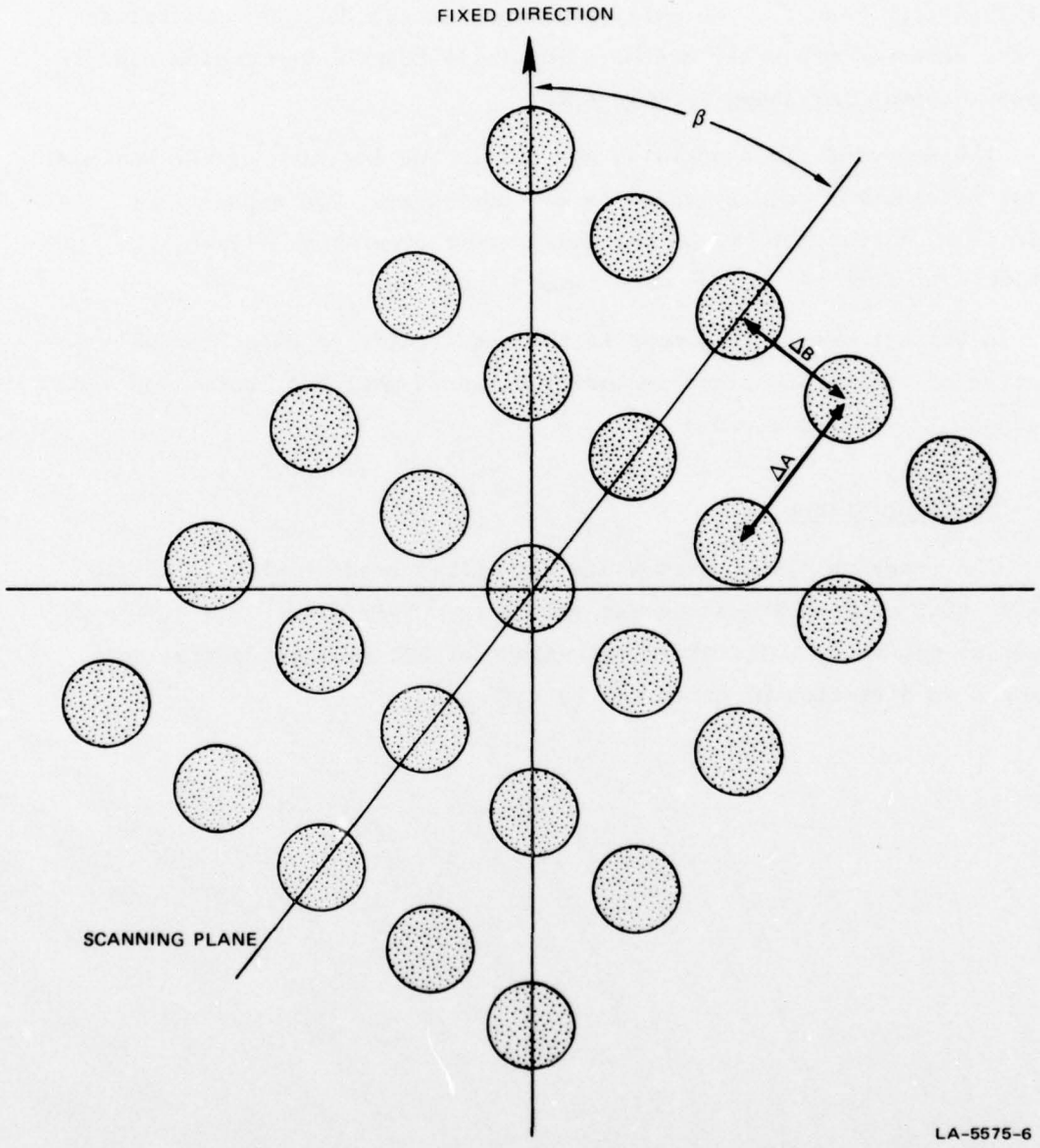

FIGURE 12 DIFFERENT DIRECTIONS IN WHICH THE RADAR BEAM WAS POINTED DURING 1 MINUTE OF MODE 1 TRACKING — EVENT ANNE

V SEQUENCE OF OPERATIONS

The single operations performed by the radar have been progressively examined starting from the most elemental ones. This section will describe the typical sequency of operations and typical data acquired during a mission. Figure 13 shows such a sequence on a time axis.

The preliminary measurements were started as soon as the necessary hardware modifications of the radar were completed and the computer programs loaded. The first operation performed was to obtain a receiver response or calibration curve that was stored in the memory and recorded for later use. The calibration of the radar took about 3 minutes. The next step was to obtain an ionosphere profile while the antenna beam was pointed straight up. This ionosphere run, which took about 3 minutes, was compared with ionosonde measurements of the critical frequency of the F-layer. The third operation was another 3-minute ionosphere run with the antenna beam pointing at the nominal release point. This last ionosphere run was used to correct the measurements for ionosphere background or to calculate the quantities W_i in Figure 4.

The same sequence of calibration and ionosphere runs was repeated at the end of the mission when the track was terminated.

When the payload rocket was launched, the radar waited 100 s and then an acquisition fence was set to find and track the rocket. The rocket was followed up to the nominal release time and the Kalman filter was initialized with that position.

For 30 s after release, rough data were acquired on a pulse-by-pulse basis with the antenna beam stationary. These data are only for later analysis and are expected to give insight into the fast ionization process that takes place in the first 20 to 30 s.

After the first 30 s, a Mode II 5-by-5-position scan started the actual tracking process. A sequence of 18 Mode I planes was done next, followed by another 5-by-5-position Mode II scan.

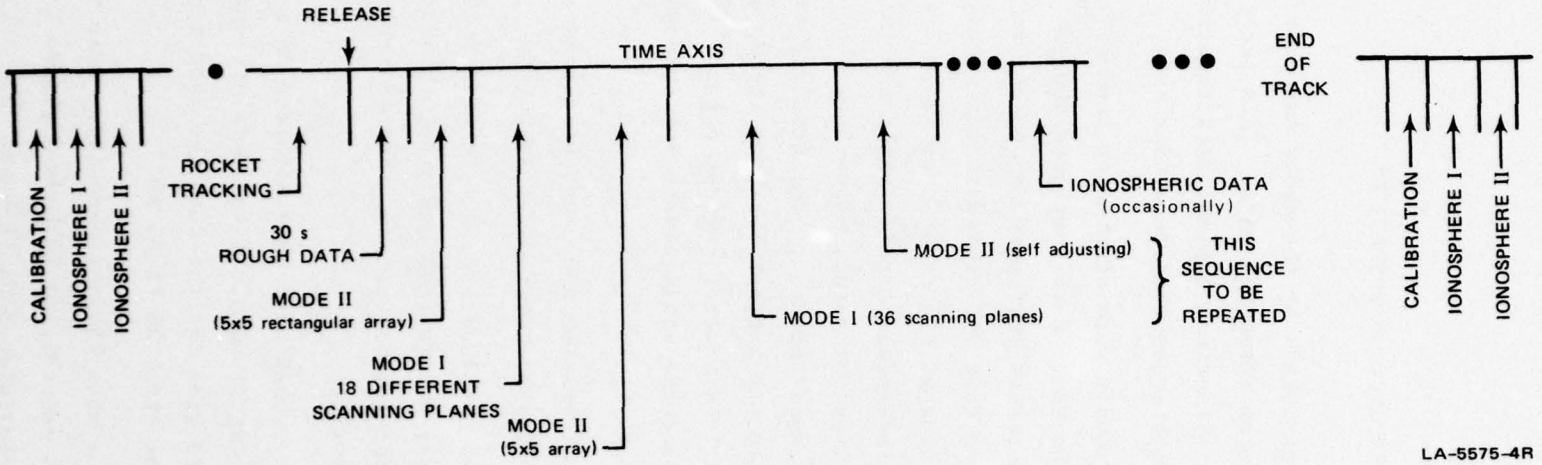

FIGURE 13 ION-CLOUD TRACKING SEQUENCE

After the second Mode II scan was made, we continued a normal sequence of operations that consisted of 36 Mode I planes followed by a self-adjusting Mode II rectangular scan.

Occasionally, 10-to-15-s ionosphere runs were made by moving the beam 15° in azimuth and at the same elevation as the center of the cloud. These ionosphere runs were made to update the ionosphere profiles used in the correction of the data.

The normal sequence of operations could be disrupted at any time by manual command. The computer program also had a feature that would allow the normal sequence of operations to occur, except the measured cloud positions were not used by the Kalman tracking filter. This feature was used when the probe rockets were fired, so that the tracking filter would not be allowed to follow these rockets.

VI PRELIMINARY RESULTS

A. Pre-STRESS Release (Event ANNE)

At the time of the Pre-STRESS release the AN/FPS-85 radar was operational and the software had been completed by Bendix according to specifications provided by SRI. Four minutes before rocket firing there was a computer malfunction that caused the display screen to go blank. Fortunately, the disruption was located and resolved without delaying the operation.

At the time of rocket firing, the signal was given to the computer that caused the radar to set a fence to acquire the payload rocket within 100 s after launch. This intended acquisition was not accomplished, however, and at the release time (2311:43 UT) the radar was pointed at the nominal release point for the first 30 s of rough data acquisition. No satisfactory explanation for the failure to acquire the payload rocket has been found; however, the failure did not occur again.

The release did not take place at the nominal point, so the first 30 s of rough data are not expected to yield significant results. After 30 s, the radar started scanning in a 5-by-5-position rectangular grid pattern for 25 s. Part of the cloud was in the beam in at least four positions. However, this information was not used for tracking purposes because it failed to pass one of the safety tests that were included as a safeguard against interference or spurious targets.

The first "valid" measurement was made 2 min 18 s after release, where "valid" means that the data passed the safety tests, and the tracking filter was set in motion. From this time until the radar was returned to Air Force control over three hours later, a steady track of the cloud or a portion of the cloud was maintained.

Steady spike-like signals in the radar returns proved to be extremely troublesome during the tracking of the ion cloud. This interference was

particularly strong, and at the same range as the cloud, around R + 1 hr 14 min, R + 2 hr 13 min, and R + 2 hr 20 min. It also appeared in lesser degree at various other times.

One of the data-valid safety tests prevented tracking of the densest part of the cloud, since this test disallowed the use of some good data points as "valid" measurements for the tracking filter. This problem was corrected for subsequent events.

Figure 14 shows the motion of the tracked point. After the first 20 min, the mean velocity of the cloud was 17.5 m/s at an azimuth of 164°. The initial velocity was in the order of 20 m/s to the east, although this velocity is less well defined since it is subject to the initial cloud-position measurement fluctuations. The excursion that appears between R +2 hr and R +2 hr 20 min is due to interference rather than to cloud motion.

Figure 15 shows the altitude history of the tracked portion of the cloud. At this time, altitude is not a well defined parameter, since the vertical dimension of cloud is expected to be about 30 km. Further analysis of the data is expected to be more explicit in defining the cloud height.

Figure 16 shows the preliminary electron density of the cloud where the numbers have been chosen judiciously from the returns to weed out interference and to select the densest portions of the cloud illuminated by the radar. The data points marked by large dots are questionable. It has not been determined whether they represent valid density measurements or interfering signals. Figure 17 repeats the same data in a logarithmic time scale. The theoretical curve (smooth line) of maximum electron density has also been included for comparison with measured data.

B. STRESS Series

After Event ANNE, corrective measures were implemented for the later tests, particularly to alleviate the interference problem. The main data will be presented below, with a few comments about each event.

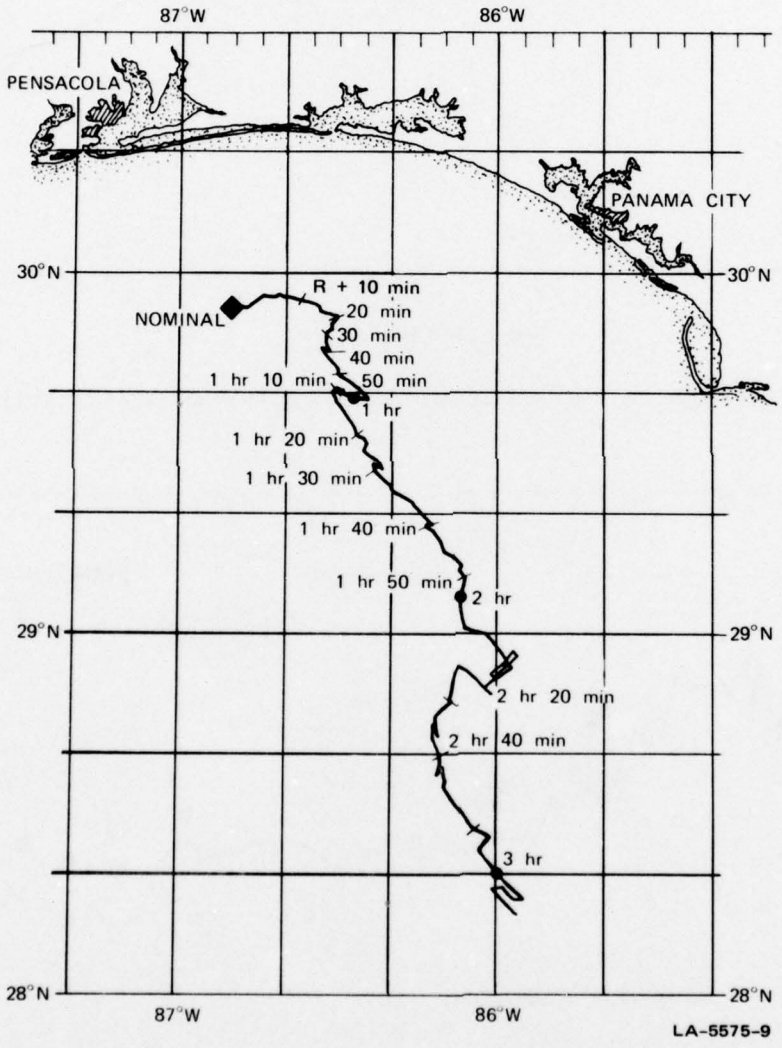

FIGURE 14 CLOUD MOTION — EVENT ANNE

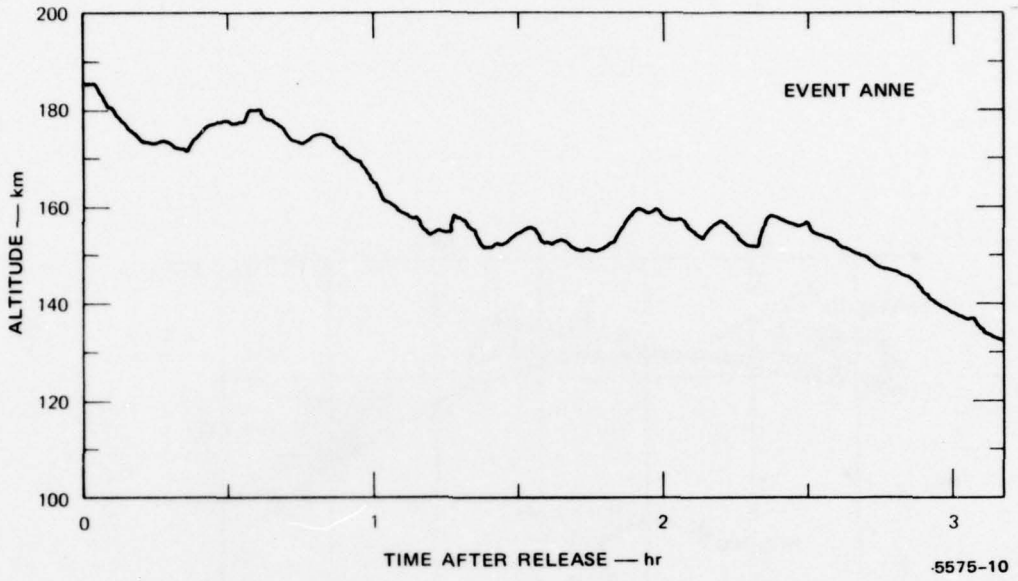

FIGURE 15 ALTITUDE OF THE ION CLOUD AS A FUNCTION OF TIME — EVENT ANNE

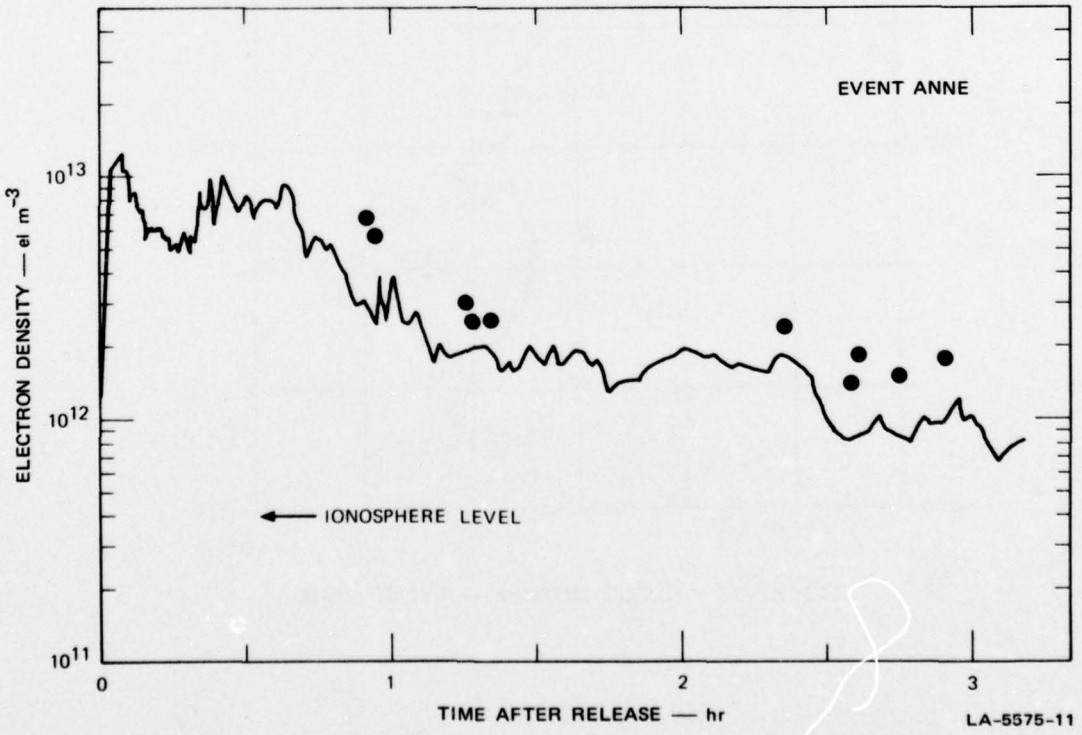

FIGURE 16 APPROXIMATE ELECTRON DENSITIES — LINEAR SCALE OF TIME, EVENT ANNE

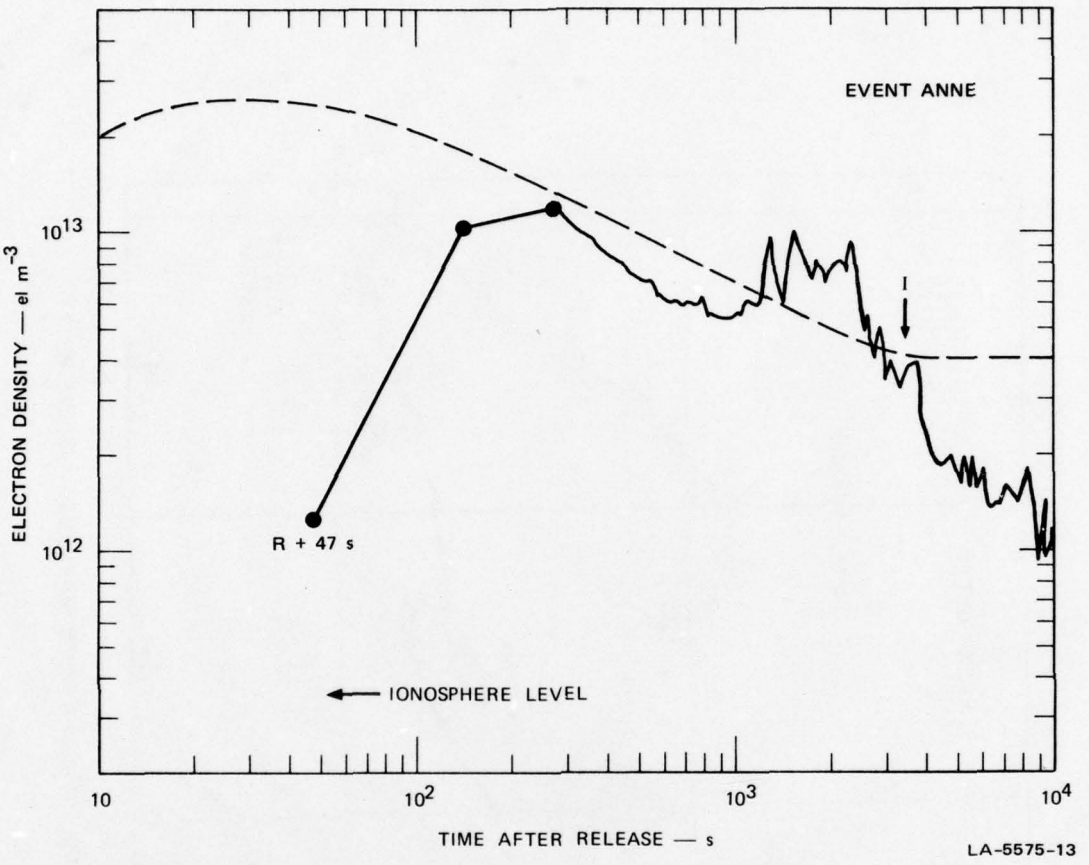

FIGURE 17 APPROXIMATE MAXIMUM ELECTRON DENSITY — LOGARITHMIC SCALE OF TIME, EVENT ANNE

1. Event BETTY

The history of the ion cloud is presented in Figures 18 through 21. The ion cloud was lost 3 min after release and briefly reappeared at R +15 min, and the regular track was well established at R +45 min. At R +1 hr 45 min, the motion of the track of the cloud reversed for 15 minutes and reversed again parallel to the earlier direction. It is believed that the tracked point shifted from one point of the ion cloud to another in this period of time.

The track became erratic after R + 2 hr 50 min, and tracking was terminated at R + 3 hr 10 min.

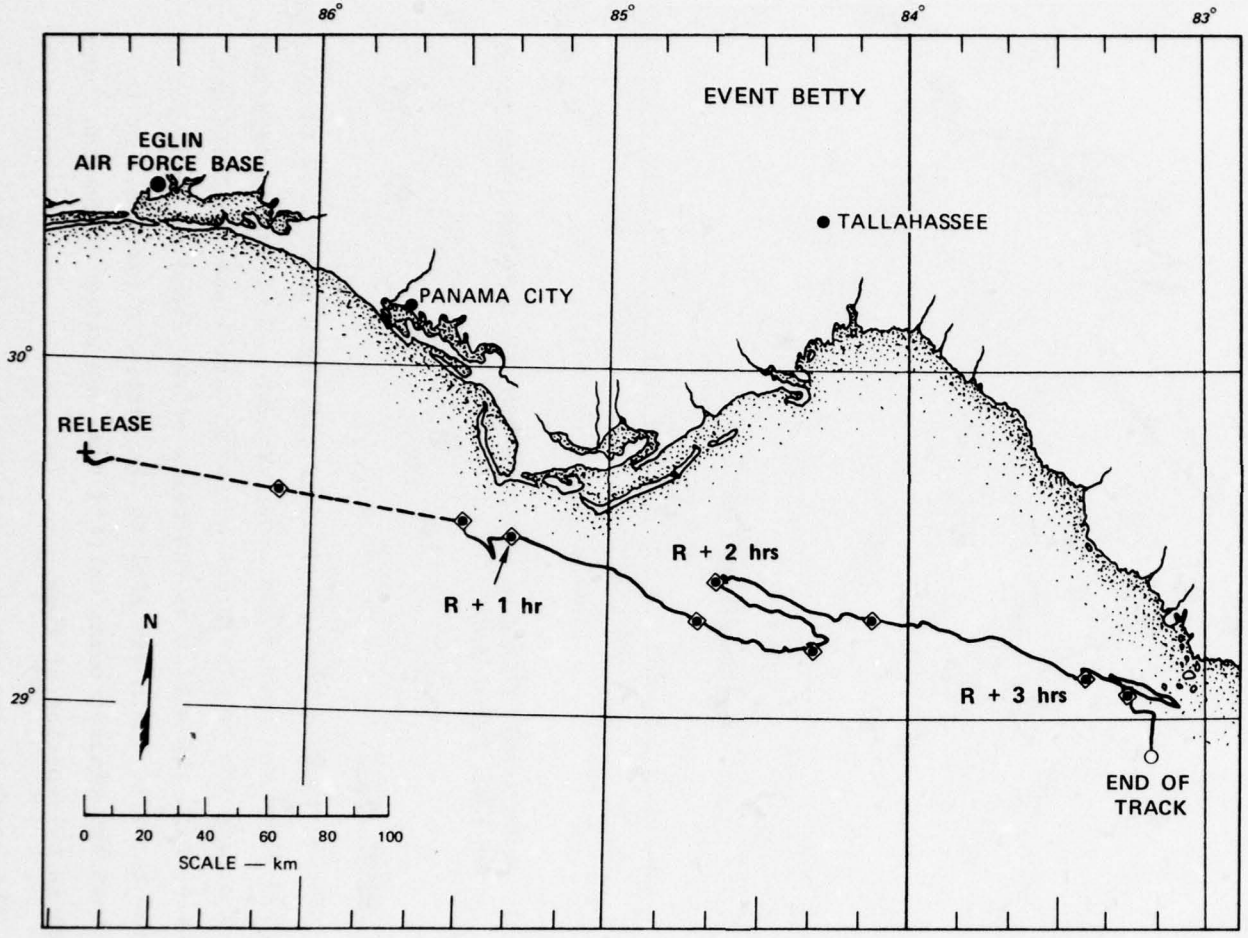

FIGURE 18 MOTION OF ION CLOUD WITH 20-MINUTE MARKERS — EVENT BETTY

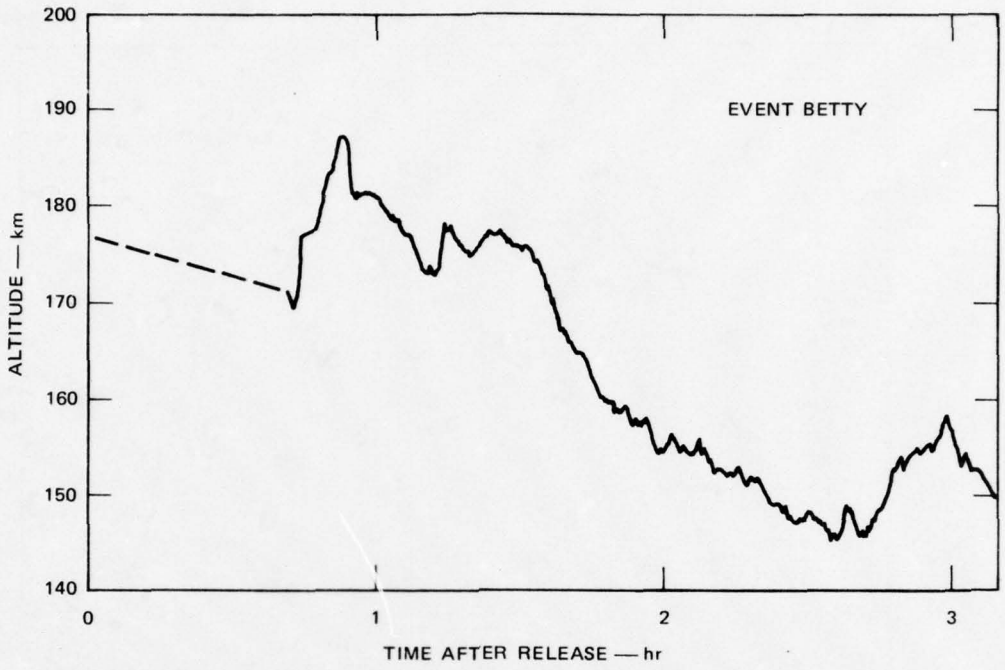

FIGURE 19 ALTITUDE OF ION CLOUD AS A FUNCTION OF TIME — EVENT BETTY

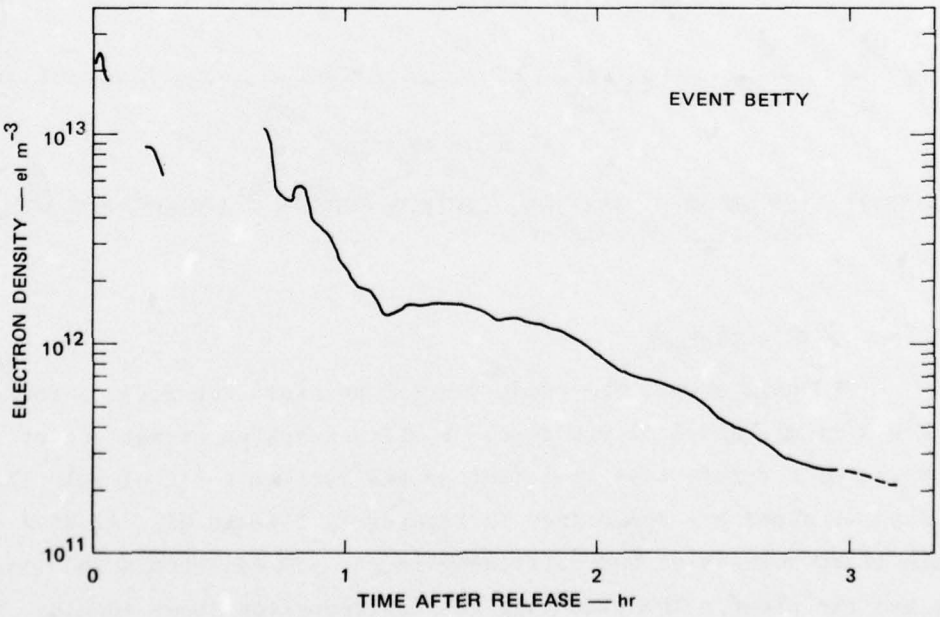

FIGURE 20 APPROXIMATE ELECTRON DENSITIES — LINEAR SCALE OF TIME, EVENT BETTY

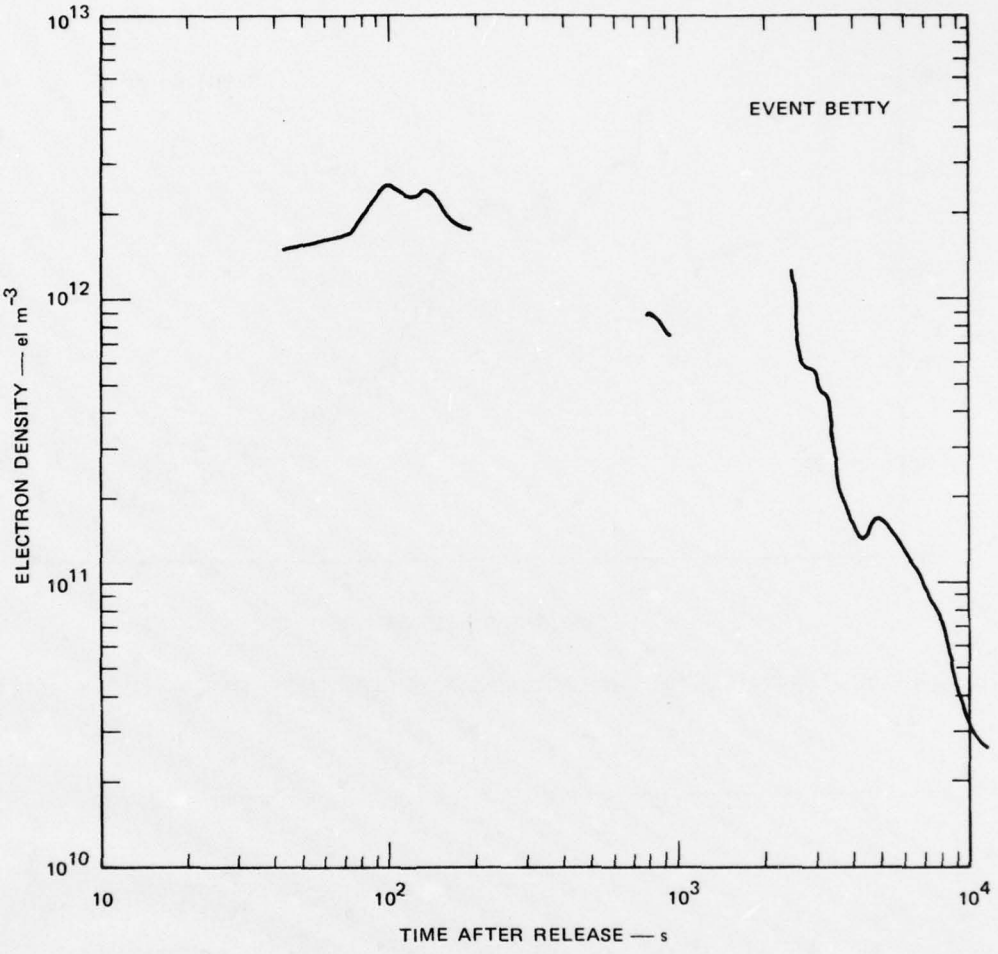

FIGURE 21 APPROXIMATE MAXIMUM ELECTRON DENSITY — LOGARITHMIC SCALE OF TIME, EVENT BETTY

2. Event CAROLYN

In this event, the radar started to track the payload rocket between R +1 min and R +1 min 15 s. Further tracking of the rocket was prevented by a safety test that limited the maximum vertical velocity. The data obtained are summarized in Figures 22 through 25. At R +1 hr 46 min after release we had difficulty in the A/D converters and lost data and the cloud. The cloud was re-acquired after about 10 min. The cloud became erratic at about R +2 hr 20 min as it approached the limits of coverage of the radar. Track was terminated at R +2 hr 55 min.

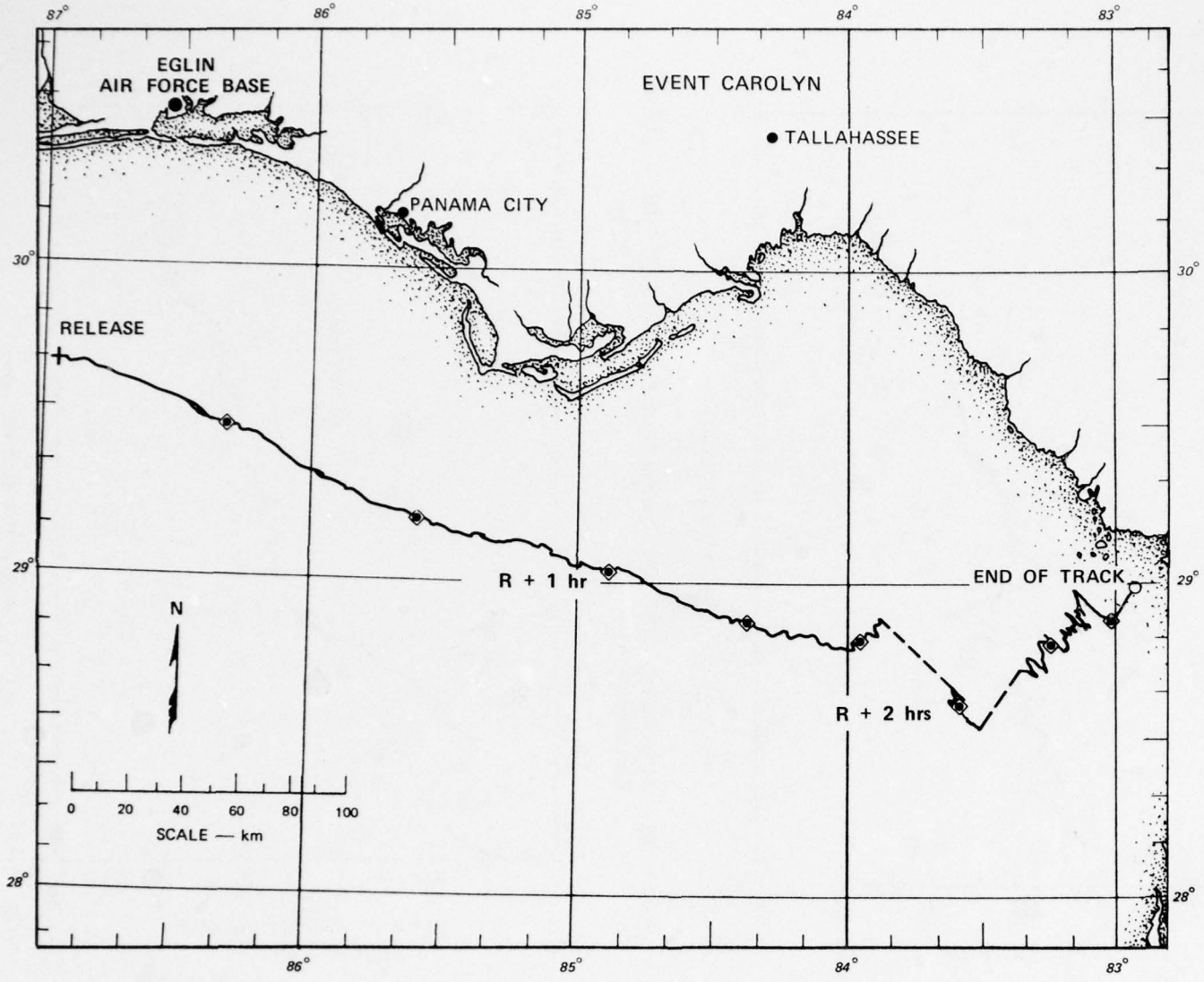

FIGURE 22 MOTION OF ION CLOUD WITH 20-MINUTE MARKERS — EVENT CAROLYN

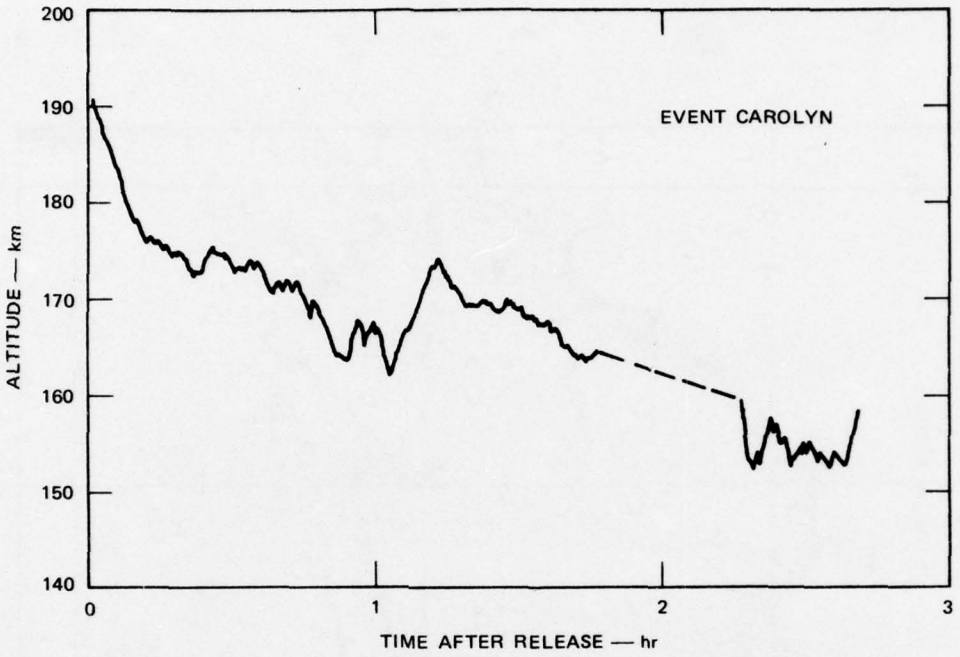

FIGURE 23 ALTITUDE OF THE ION CLOUD AS A FUNCTION OF TIME — EVENT CAROLYN

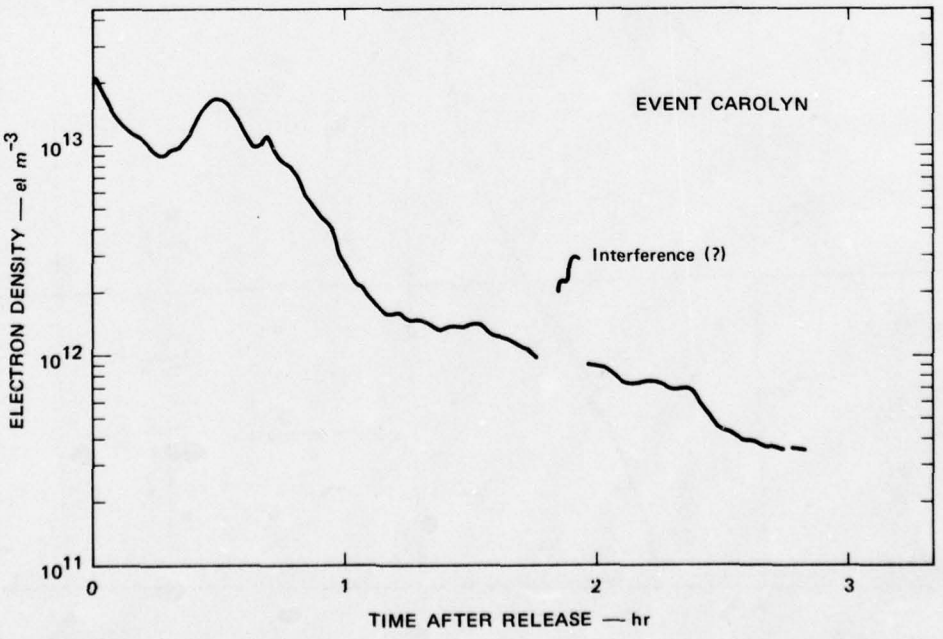

FIGURE 24 APPROXIMATE ELECTRON DENSITIES — LINEAR SCALE OF TIME, EVENT CAROLYN

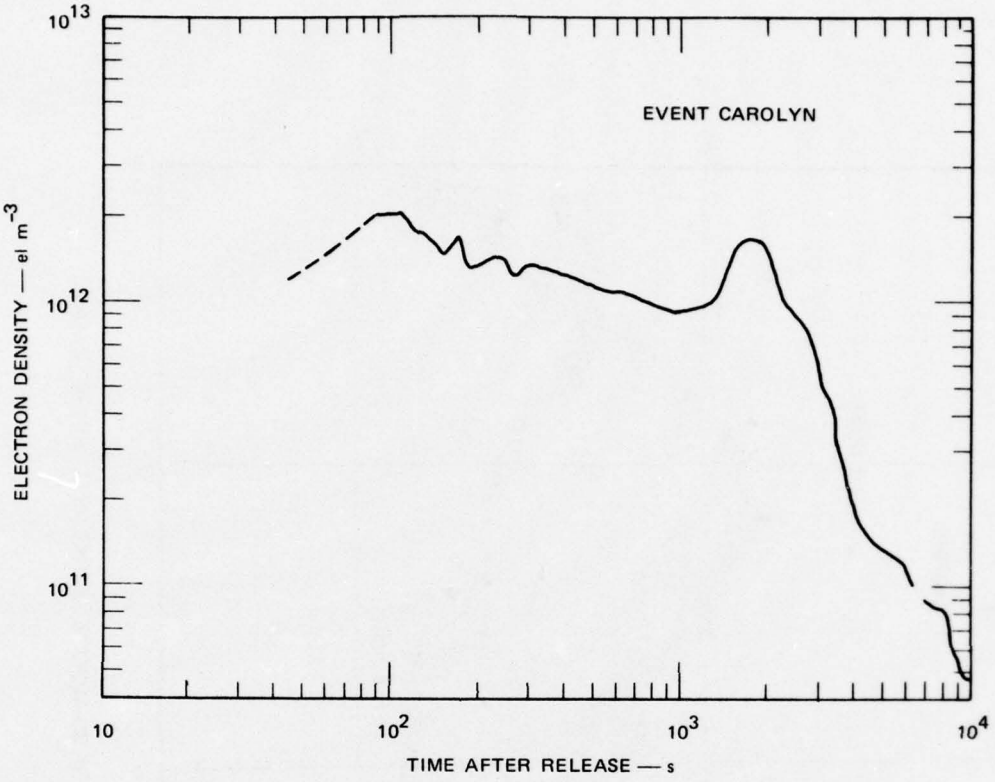

FIGURE 25 APPROXIMATE MAXIMUM ELECTRON DENSITY — LOGARITHMIC SCALE OF TIME, EVENT CAROLYN

3. Event DIANNE

The data for Event DIANNE are shown in Figures 26 through 29. The cloud track was lost at R +15 min and re-acquired at R +39 min. Throughout the tracked period the motion of the cloud seems noisier and more erratic than in the previous events, and a change of sense of the north-south component of motion can be seen in Figure 26. The track was terminated at R +2 hr 55 min..

4. Event ESTHER

The data of Event ESTHER are presented in Figures 30 through 33. The track of the cloud was very good for at least 3 hours. At R +3 hr 30 min the track was suspected of sidelobe contamination and the radar was reset manually. The track became erratic after this time.

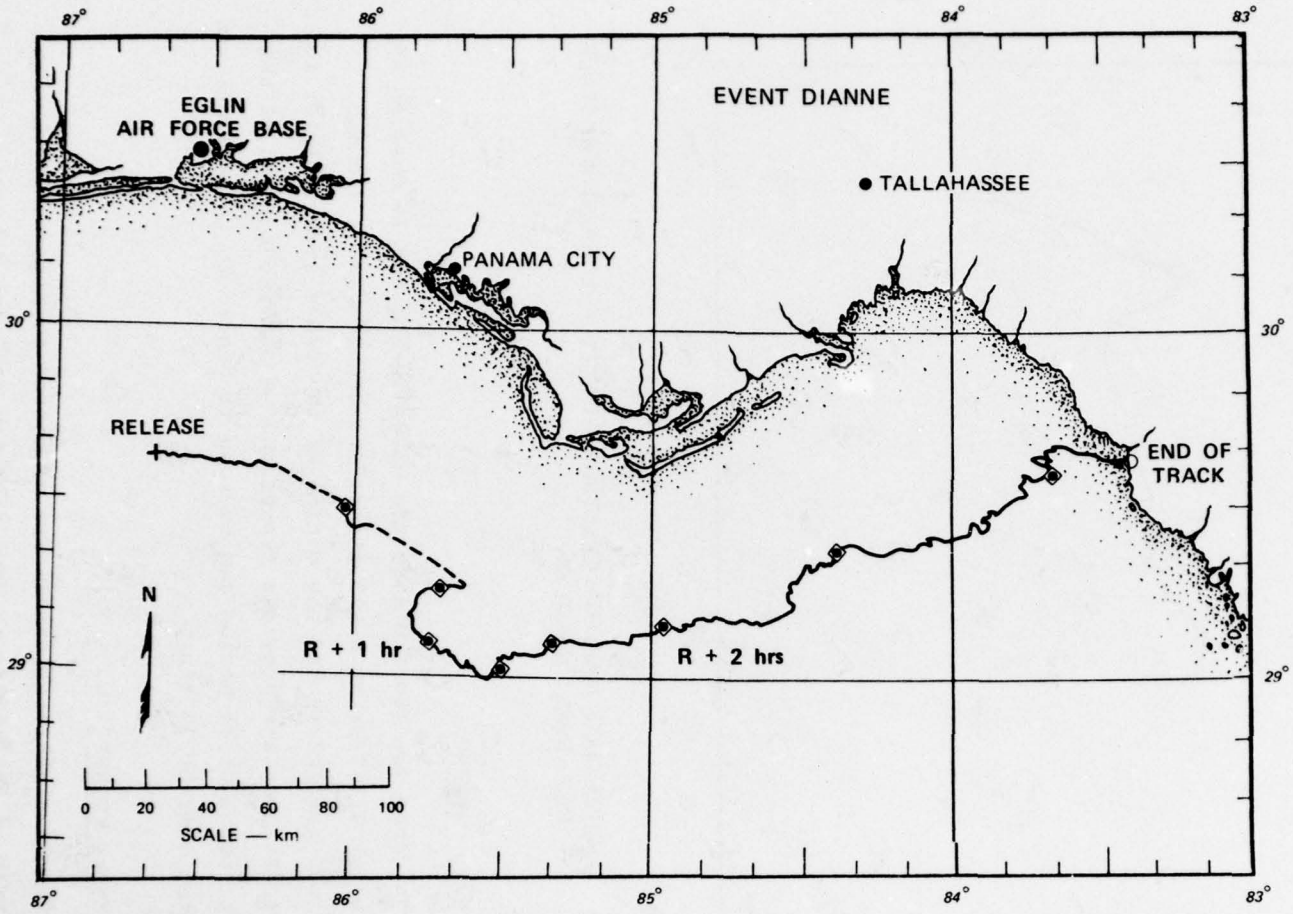

FIGURE 26 MOTION OF ION CLOUD WITH 20-MINUTE MARKERS — EVENT DIANNE

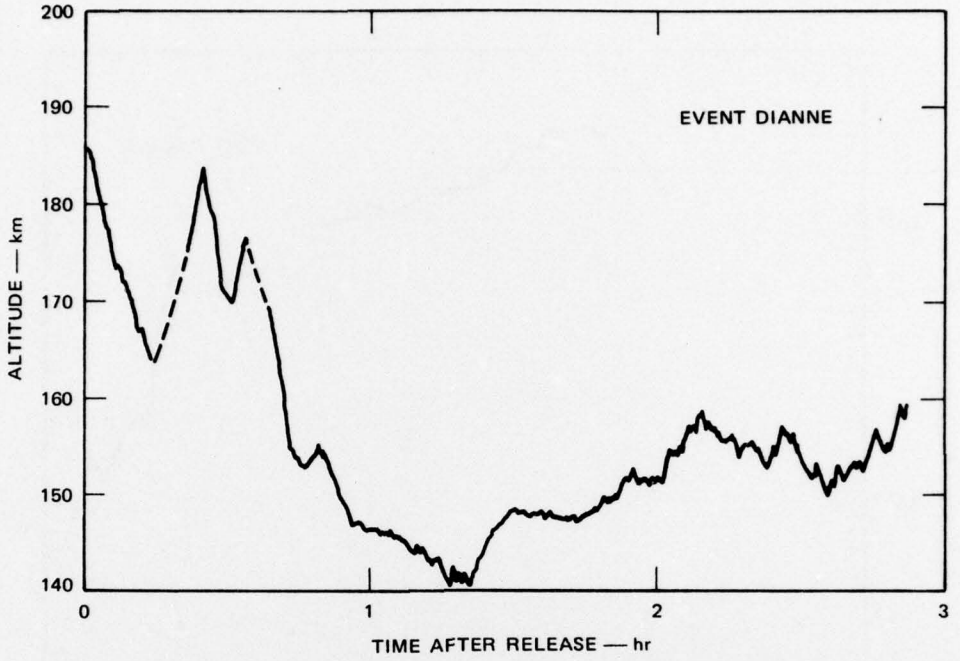

FIGURE 27 ALTITUDE OF THE ION CLOUD AS A FUNCTION OF TIME — EVENT DIANNE

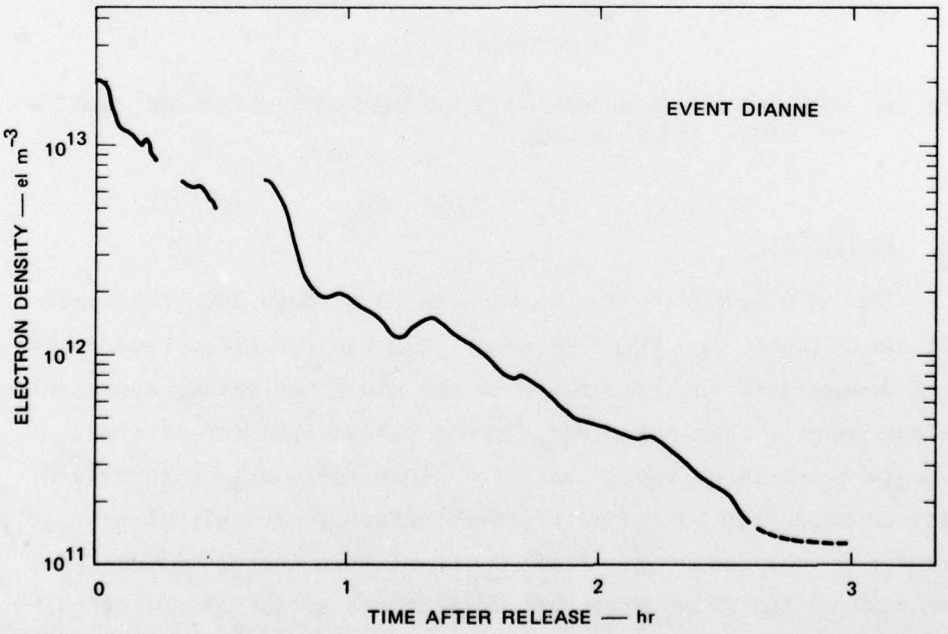

FIGURE 28 APPROXIMATE ELECTRON DENSITIES — LINEAR SCALE OF TIME, EVENT DIANNE

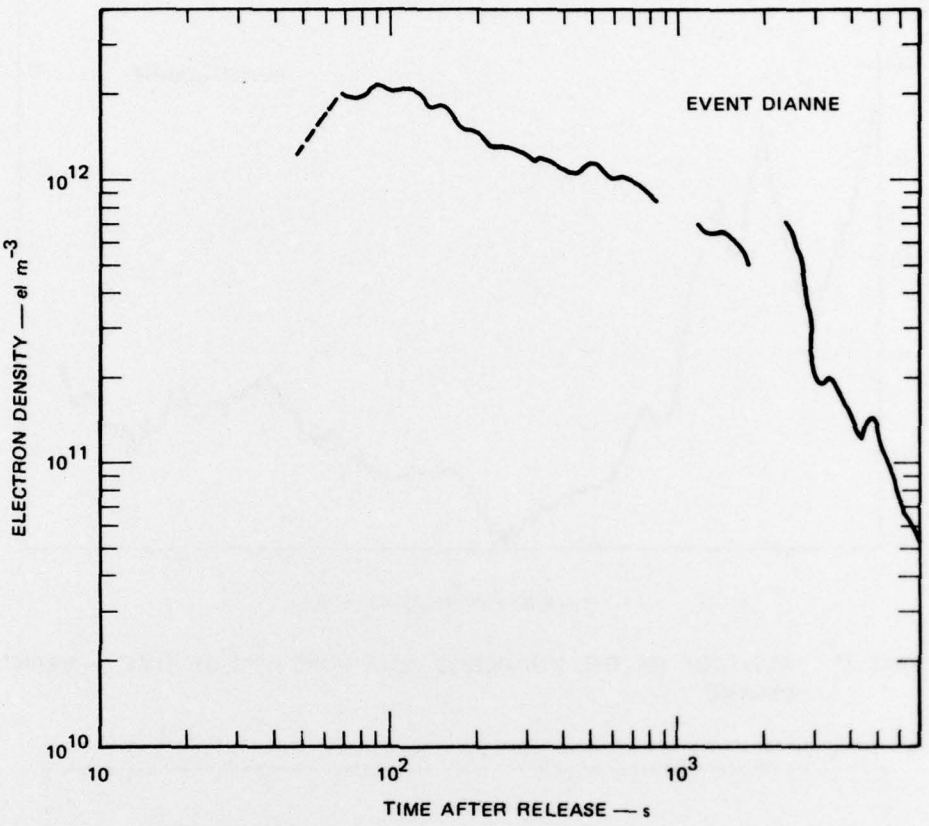

FIGURE 29 APPROXIMATE MAXIMUM ELECTRON DENSITY LOGARITHMIC SCALE OF TIME — EVENT DIANNE

5. Event FERN

The data are presented in Figures 34 through 37. The track was well established soon after release. The cloud drifted toward the radar and downward so that the range to the cloud decreased, approaching our minimum range. Simultaneously, strong echoes appeared at close ranges where the E-layer should be. The close range echoes increased gradually in intensity to the point of interfering strongly with the cloud data and the normal tracking. After R +40 minutes the motion of the cloud as seen by the radar might not reflect the motion of the actual cloud because the whole tracking procedure was extremely degraded by the echoes at E-layer ranges. Figure 38 shows examples of the gradual onset of these echoes.

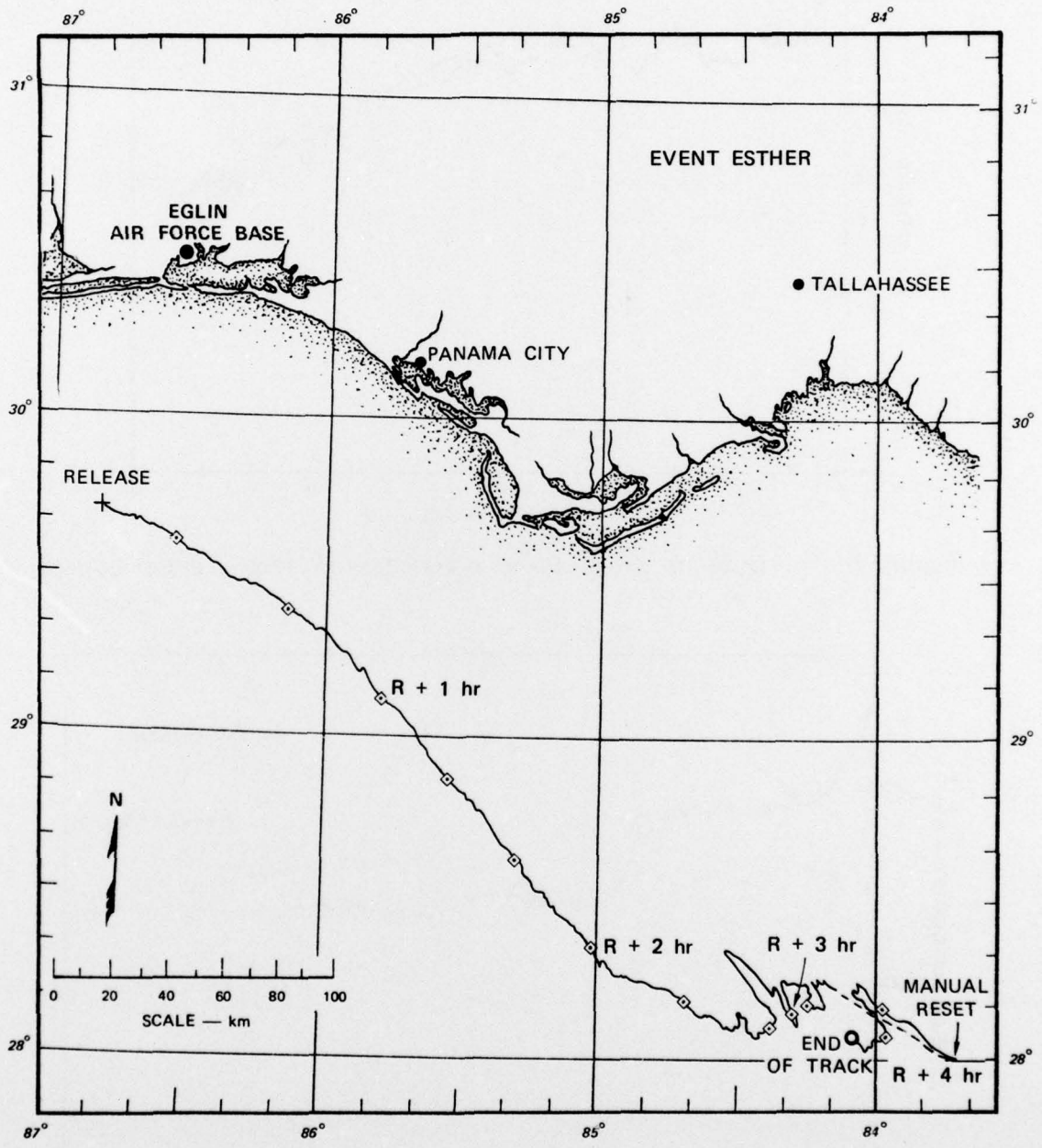

FIGURE 30 MOTION OF ION CLOUD WITH 20-MINUTE MARKERS — EVENT ESTHER

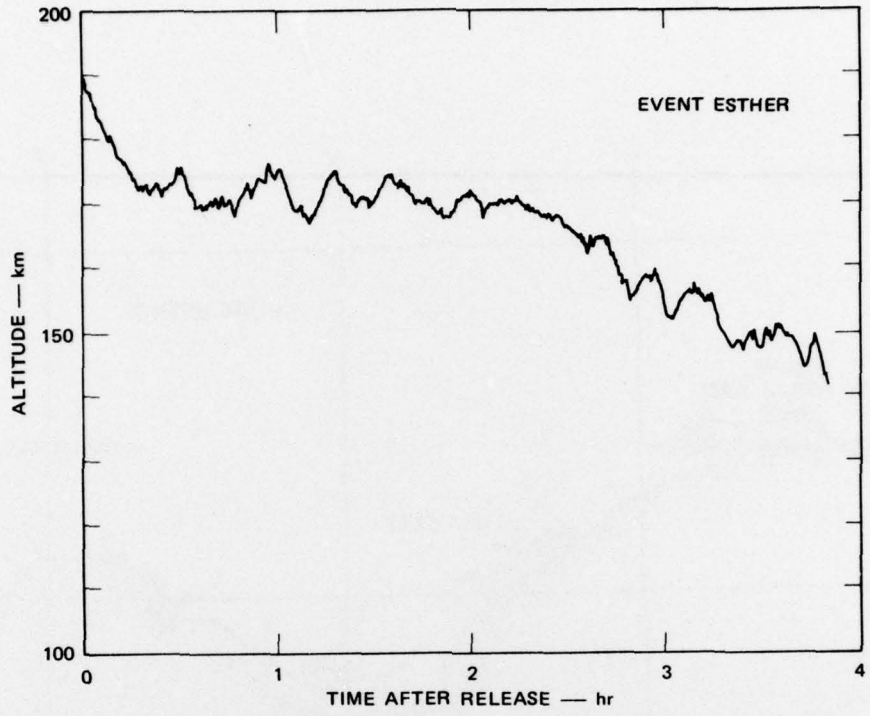

FIGURE 31 ALTITUDE OF ION CLOUD AS A FUNCTION OF TIME — EVENT ESTHER

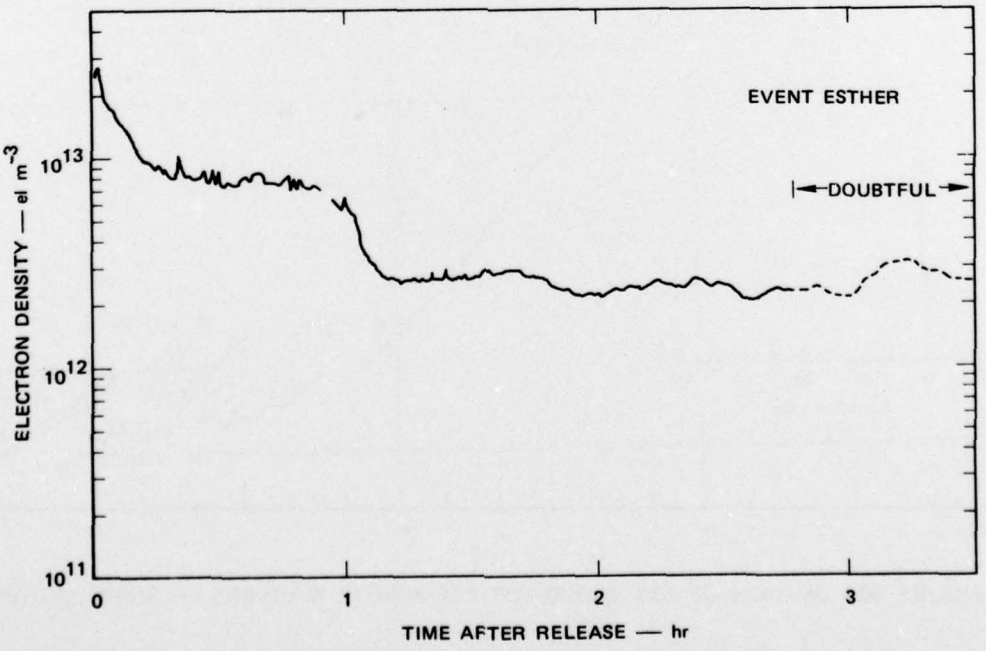

FIGURE 32 APPROXIMATE ELECTRON DENSITIES — LINEAR SCALE OF TIME, EVENT ESTHER

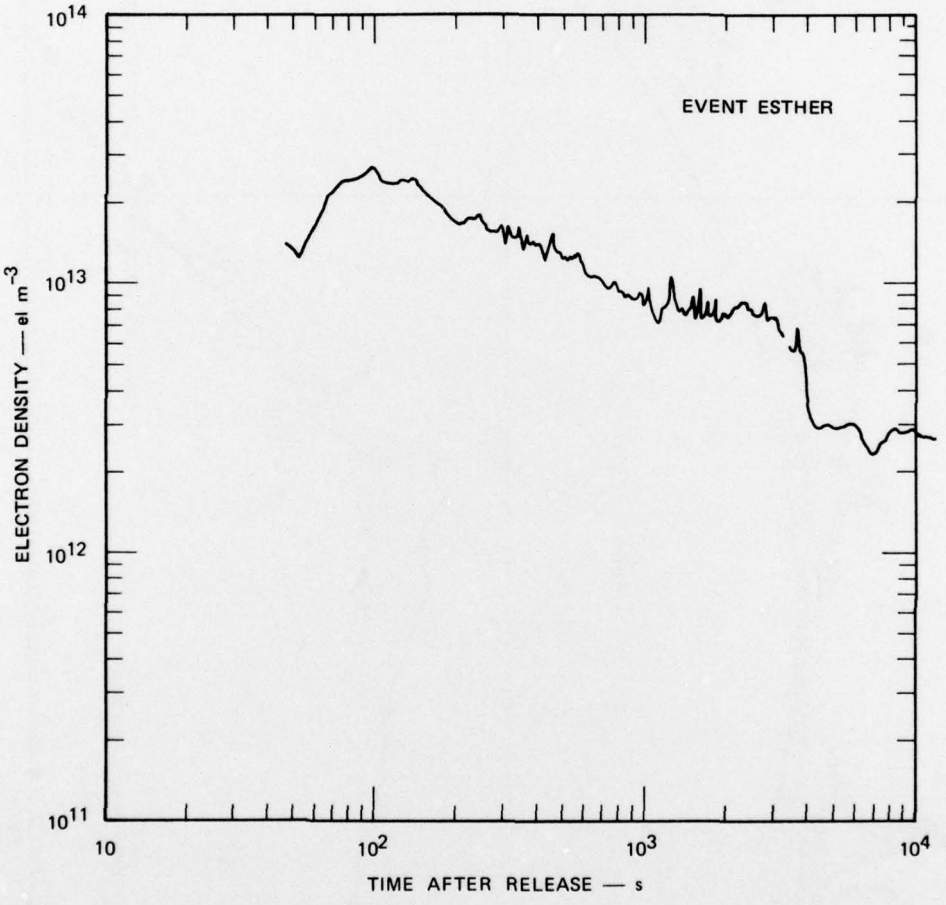

FIGURE 33 APPROXIMATE MAXIMUM ELECTRON DENSITY — LOGARITHMIC SCALE OF TIME, EVENT ESTHER

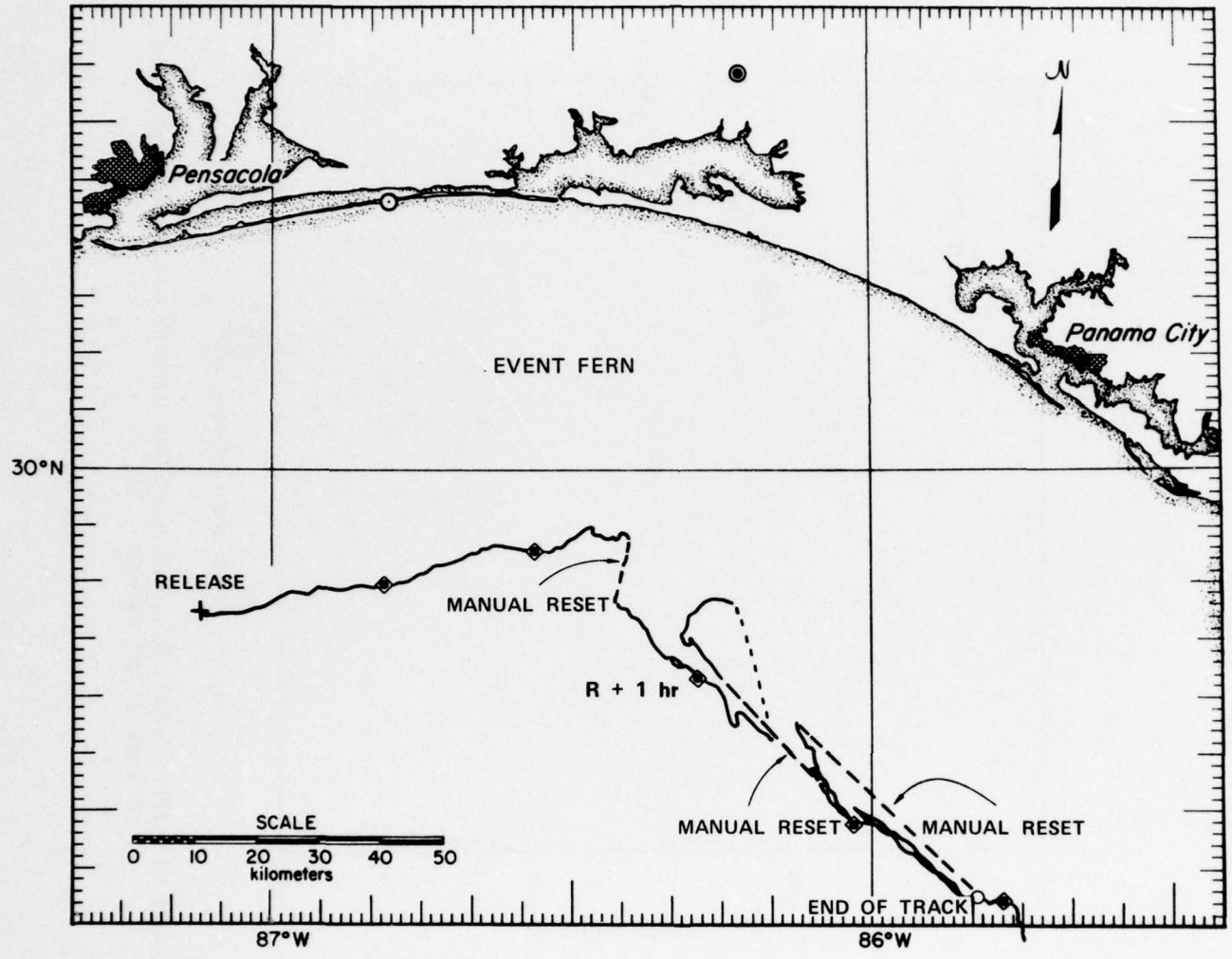

FIGURE 34 MOTION OF ION CLOUD WITH 20-MINUTE MARKERS — EVENT FERN

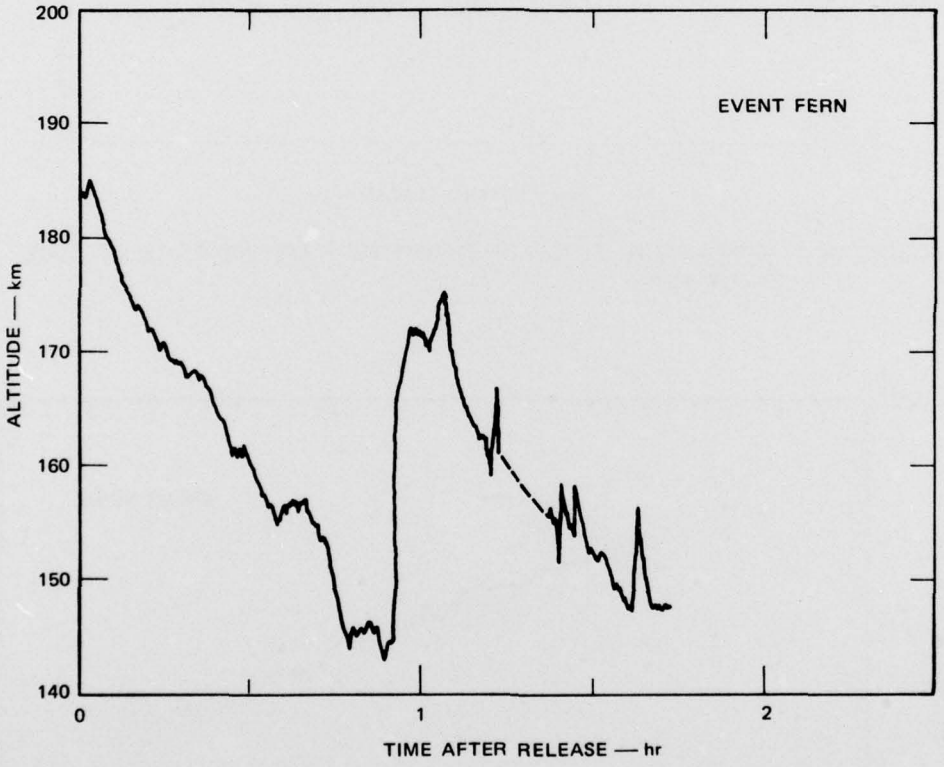

FIGURE 35 ALTITUDE OF ION CLOUD AS A FUNCTION OF TIME — EVENT FERN

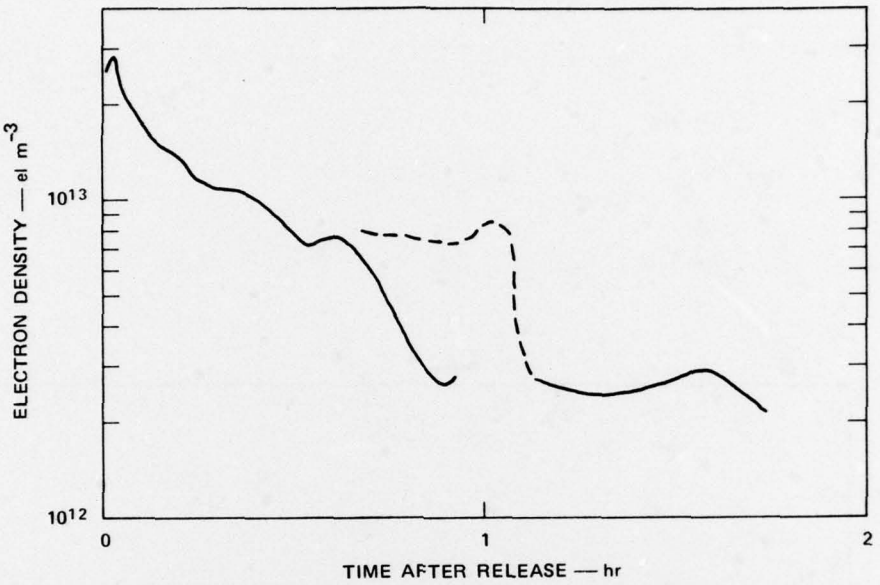

FIGURE 36 APPROXIMATE ELECTRON DENSITIES — LINEAR SCALE OF TIME, EVENT FERN

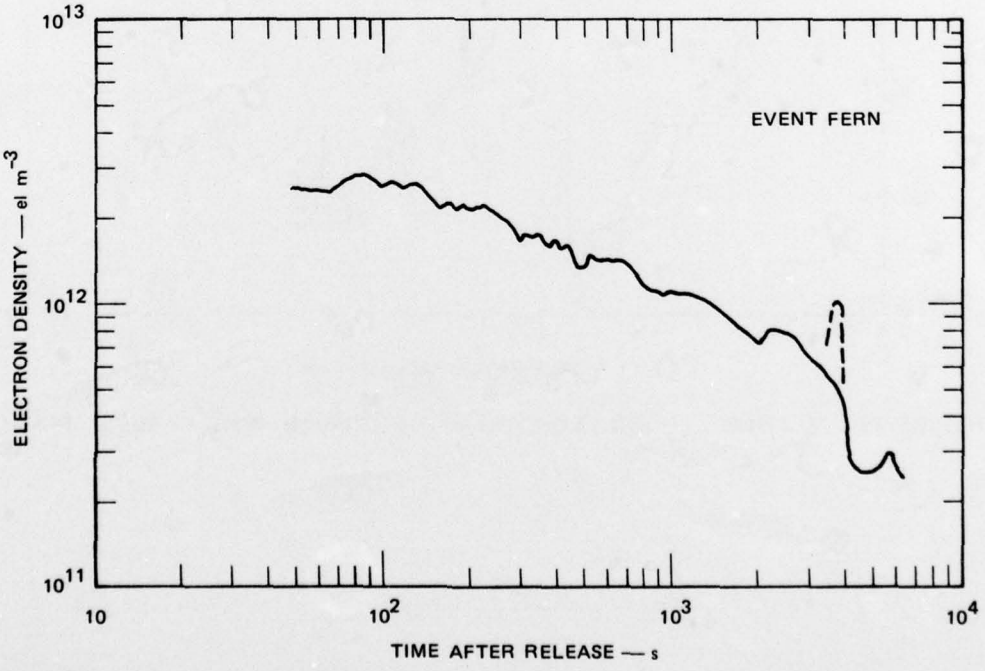

FIGURE 37 APPROXIMATE MAXIMUM ELECTRON DENSITY — LOGARITHMIC SCALE OF TIME, EVENT FERN

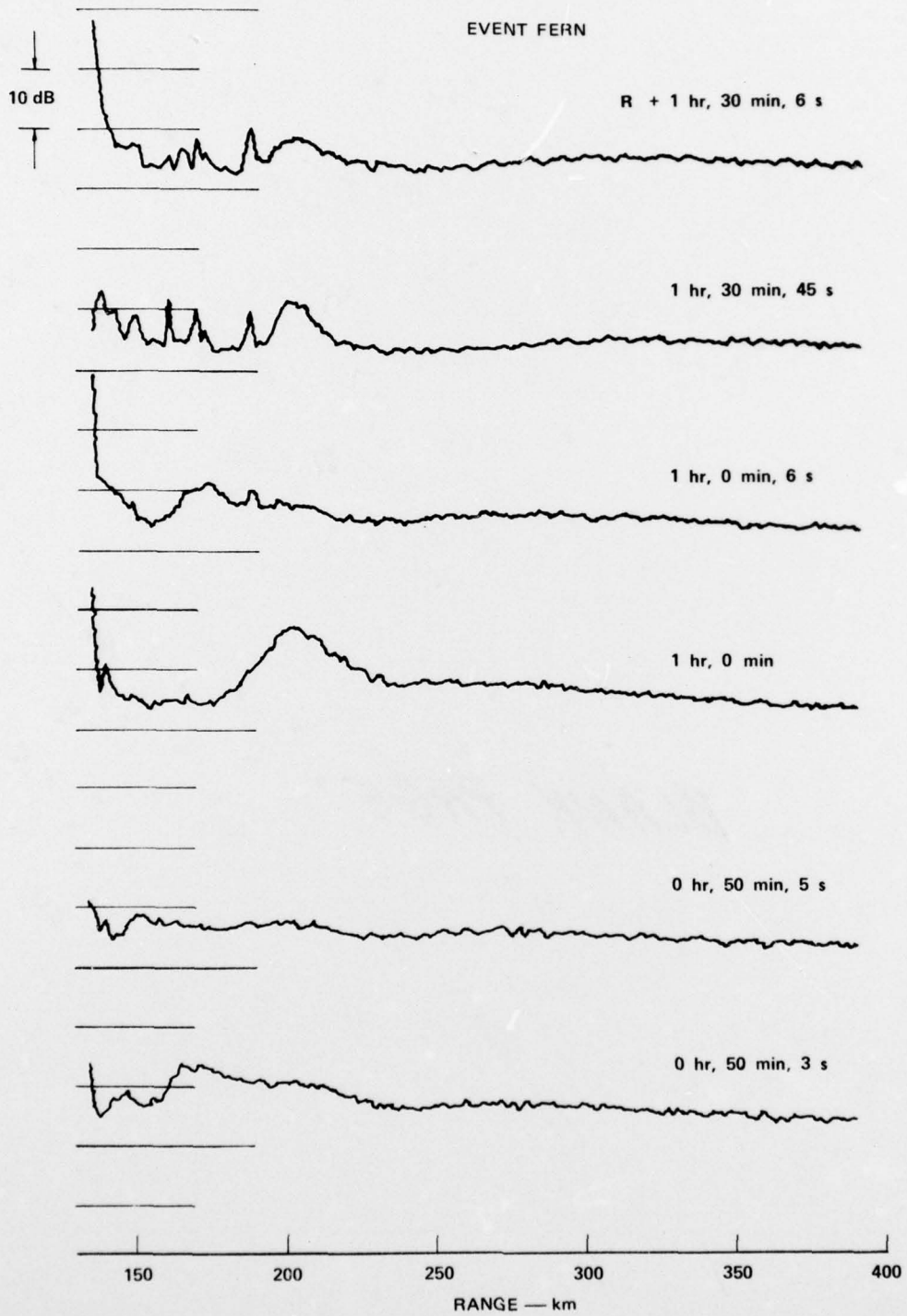

FIGURE 38 RECORDED DATA POWER RETURNED AS A FUNCTION OF RANGE AT VARIOUS TIMES — EVENT FERN

VII CONCLUSIONS

The tracking of Ba-ion clouds by use of the incoherent-scatter technique was accomplished successfully for the first time. When reviewing the overall performance of the ion-cloud tracking process we should evaluate (1) the performance of the real-time data processing, the tracking algorithm, and the protective tests, (2) the effectiveness of the automatic decisions versus that of the manual decisions, and (3) the information available to the radar operator to appraise the quality of the track. Finally, we should also examine the single case in which the basic tracking logic was degraded due to behavior of the cloud itself.

The real-time data processing was adequate and probably optimum for the AN/FPS-85. The addition of a sanitation routine that cancelled narrow peaks from the return was very successful and took care of most of the difficulties.

The Mode I scanning and tracking performed extremely well, even better than was expected during the planning stages. Some of the favorable characteristics of Mode I were not discovered until after Event ANNE. The time response of Mode I was very short, compared to that of Mode II. The Mode II scanning was quite useful in acquiring cloud profiles, but it added little to the normal tracking procedure. It was expected that the duration of the tracking time could be extended by working with smaller electron densities than in Mode I, but this expectation has not been validated. The second planned use of Mode II was to search for the ion cloud when it was lost, but this search process proved to be very difficult. If the need of tracking an ion cloud arises again, it would be desirable to plan a specialized search mode.

Reviewing the performance of the overall tracking algorithm, we may say that the chain of automatic decisions and protective tests involved in the tracking process performed extremely well. On the occasions when the ion cloud was lost, it was due either to equipment or operator failure.

The procedures to reacquire the ion cloud by manual operation of the radar were cumbersome and time-consuming, and sometimes the safety tests that were included to assure the quality of the automatic track defeated the efforts to reacquire the ion cloud.

The problems of reacquiring an ion cloud when lost, and of tracking a late-time cloud are related to one common factor: operator feedback. The information available to the operator about the quality of the track was limited because the output devices of an operational radar such as the AN/FPS-85 are somewhat rigid in uses for which they were not originally intended. Two main modes of monitoring the track of the cloud existed. The first was the use of an A-scope that displayed the detected signal; this mode was useful at early times to determine whether the ion cloud was or was not illuminated by the antenna beam. At later times, the returns from an ion cloud were not visible in the scope (although the data were expected to be usable through integration), and this mode of feedback was no longer useful. The second mode of feedback was the use of the printer to print numbers in a map-like array to display Mode II returns. This mode was slow and it was dependent on the choice of numbers that were printed. The evaluation of this feedback mode still remains to be completed by comparing the recorded detailed data with the decisions made in the field. In the field we had some difficulty deciding when to terminate the track after the data became marginal in quality.

The plotting of the motion of the cloud from the printed values may itself be considered a third mode of feedback. When the track became erratic, it was assumed to be bad. This assumption will be refined during the post-experiment data analysis.

Finally, we can say that the event whose development degraded the tracking logic was FERN. This one release out of six is thought to be responsible for strong echoes appearing at close ranges that ultimately defeated the automatic tracking procedure at very early times (R +1 hr 30 min). This event, interesting as it is by itself, raises two questions if future missions are to be planned. One is, how frequent are the physical conditions that might result in a repeat situation, and the second

is whether or not it is possible to solve the tracking problems by more sophisticated data processing. We believe that the analysis of the data will answer the second question in the affirmative.

DISTRIBUTION LIST

DEPARTMENT OF DEFENSE

Assistant Secretary of Defense
Cmd., Cont., Comm., & Intell.
ATTN: J. Babcock
ATTN: M. Epstein

Director
Defense Advanced Rsch. Proj. Agency
ATTN: Strategic Tech. Office

Director
Defense Communications Agency
ATTN: Code 101B, Major Rood
ATTN: Code 810, R. W. Rostron

Defense Communications Agency
WWMCCS System Engineering Org.
ATTN: R. L. Crawford

Defense Documentation Center
Cameron Station
12 cy ATTN: TC

Under Secretary of Def. Rsch. & Engrg.
ATTN: S&SS (OS)

Director
Defense Nuclear Agency
ATTN: DDST
ATTN: TISI, Archives
3 cy ATTN: TITL, Tech. Library
3 cy ATTN: RAAE

Commander
Field Command
Defense Nuclear Agency
ATTN: FCPR

Chief
Livermore Division Fld. Command DNA
Lawrence Livermore Laboratory
ATTN: FCPRL

DEPARTMENT OF THE ARMY

Commander
Harry Diamond Laboratories
ATTN: DRXDO-NP, Francis N. Wimenitz
ATTN: DRXDO-TI, Mildred H. Weiner

Commander
U.S. Army Electronics Command
ATTN: DRSEL-NL-RD, H. S. Bennet

Commander
U.S. Army Nuclear Agency
ATTN: MONA-WE, J. Berberet

Commander
U.S. Army SATCOM Agency
ATTN: Document Control

DEPARTMENT OF THE NAVY

Chief of Naval Research
ATTN: Code 461

Director
Naval Research Laboratory
ATTN: Code 7700, Timothy P. Coffey
ATTN: Code 7701, Jack D. Brown

Officer-In-Charge
Naval Surface Weapons Center
ATTN: Code WA501, Navy Nuc. Prgms. Off.

DEPARTMENT OF THE AIR FORCE

AF Geophysics Laboratory, AFSC
ATTN: PHD John P. Mullen
ATTN: PHD Jurgen Buchau

AF Weapons Laboratory, AFSC
ATTN: SUL
ATTN: DYT, Capt L. Wittwer

Air Force Avionics Laboratory, AFSC
ATTN: Allen Johnson, AAD

Headquarters USAF/RD
ATTN: RDQ

SAMSO/SK
ATTN: SKA, Lt Maria A. Clavin

DEPARTMENT OF ENERGY

Los Alamos Scientific Laboratory
ATTN: Doc. Control for John Wolcott

Sandia Laboratories
ATTN: Doc. Control for W. D. Brown, Org. 1353
ATTN: Doc. Control for T. Wright

OTHER GOVERNMENT AGENCY

Department of Commerce
Office of Telecommunications
Institute for Telecom Science
ATTN: William F. Utlaut

DEPARTMENT OF DEFENSE CONTRACTORS

Aerospace Corporation
ATTN: D. P. Olsen, 120, Rm. 2224E

Charles Stark Draper Laboratory, Inc.
ATTN: J. P. Gilmore, MS 63
ATTN: D. B. Cox
ATTN: Paul Chesnut
ATTN: David Watson

ESL, Inc.
ATTN: James Marshall
ATTN: C. W. Prettie

DEPARTMENT OF DEFENSE CONTRACTORS (Continued)

General Electric Company
TEMPO-Center for Advanced Studies
ATTN: DASIAC

JAYCOR
ATTN: S. R. Goldman

Mission Research Corporation
ATTN: R. Bogusch

R & D Associates
ATTN: Bryan Gabbard

DEPARTMENT OF DEFENSE CONTRACTORS (Continued)

The Rand Corporation
ATTN: Ed Bedrozian

Science Applications, Inc.
ATTN: D. Sachs

SRI International
ATTN: D. McDanial
ATTN: V. Gonzales